GOING BEYOND THE RANDOM PHASE APPROXIMATION: A SYSTEMATIC ASSESSMENT OF STRUCTURAL PHASE TRANSITIONS AND INTERLAYER BINDING ENERGIES

A Dissertation
Submitted to
the Temple University Graduate Board

---

in Partial Fulfillment
of the Requirements for the Degree of
DOCTOR OF PHILOSOPHY

---

by

Niladri Sengupta
August, 2018

Examining Committee Members:

Adrienn Ruzsinszky, Chair of Defense Advisory Committee, Assistant Professor, Dept. of Physics, Temple University
John P. Perdew, Chair of Defense Examining Committee, Professor, Dept. of Physics, Temple University
Qimin Yan, Member of Defense Committee, Assistant Professor, Dept. of Physics, Temple University
Spiridoula Matsika, External Member of Defense Committee, Professor, Dept. of Chemistry, Temple University

ABSTRACT

by

Niladri Sengupta

The Random Phase Approximation and beyond Random Phase Approximation methods based on Adiabatic Connection Fluctuation Dissipation Theorem (ACFD) are tested for structural phase transitions of different groups of materials, including metal to metal, metal to semiconductor, semiconductor to semiconductor transitions. Also the performance assessment of semilocal density functionals with or without empirical long range dispersion corrections has been explored for the same cases. We have investigated the structural phase transitions of three broad group of materials, semiconductor to metal transitions involving two symmetric structures, semiconductor to metal and wide bandgap semiconductor to semiconductor transitions involving atleast one lower symmetric structure and lastly special cases comprising metal to metal transitions and transitions between energetically very close structural phases. The first group contains Si (diamond $\rightarrow$ β-tin), Ge (diamond $\rightarrow$ β-tin) and SiC (zinc blende $\rightarrow$ rocksalt), second group contains GaAs (zinc blende $\rightarrow$ cmcm) and SiO_2 (quartz $\rightarrow$ stishovite) and third group contains Pb (fcc $\rightarrow$ hcp), C(graphite $\rightarrow$ diamond) and BN (cubic $\rightarrow$ hexagonal) respectively. We have found that the difference in behavior of exchange and correlation in semilocal functionals and ACFD methods is striking. For the former, the exchange potential and energy often comprise the majority of the binding described by density functional approximations, and the addition of the correlation energy and potential often induce only a (relatively) small shift from the exhcange-only results. For the ACFD, however, non self-consistent EXX typically underbinds by a considerable degree resulting in wildly inaccurate results. Thus the addition of correlation leads to very large shifts in the exchange-only results, in di-

rect contrast to semilocal correlation. This difference in behavior is directly linked to the non-local nature of the EXX, and even though the exchange-only starting point is often nowhere close to experiment, the non-local correlation from the ACFD corrects this deficiency and yields the missing binding needed to produce accurate results. Thus we find the ACFD approach to be vital in the validation of semilocal results and recommend its use in materials where experimental results cannot be straightforwardly compared to other approximate electronic structure calculations. Utilizing the second-order approximation to Random Phase Approximation renormalized (RPAr) many-body perturbation theory for the interacting density-density response function, we have used a so-called higher-order terms (HOT) approximation for the correlation energy. In combination with the first-order RPAr correction, the HOT method faithfully captures the infinite-order correlation for a given exchange-correlation kernel, yielding errors of the total correlation energy on the order of 1% or less for most systems. For exchange-like kernels, our new method has the further benefit that the coupling-strength integration can be completely eliminated resulting in a modest reduction in computational cost compared to the traditional approach. When the correlation energy is accurately reproduced by the HOT approximation, structural properties and energy differences are also accurately reproduced, as confirmed by finding interlayer binding energies of several periodic solids and compared that to some molecular systems along with some phase transition parameters of SiC. Energy differences involving fragmentation have proved to be challenging for the HOT method, however, due to errors that do not cancel between a composite system and its constituent pieces which has been verified in our work as well.

ACKNOWLEDGEMENTS

This thesis is culmination of my journey as a doctoral researcher. I am most grateful to my advisor Prof. Adrienn Ruzsinszky for her guidance and encouragement for achieving excellence in every step of this long journey. I like to thank Prof. John P. Perdew for his intellectual support and important suggestions during the course. I am also grateful to my colleague and friend Dr. Jefferson Bates (Jeb) for his enormous help, motivation and willingness to push my boundaries in this academic journey. I like to dedicate this to my parents who are my biggest inspiration now and always. I love to thank wholeheartedly my friends specially, Dr. Ka Ming Tam, Abhirup, Chandra, Niraj, Santosh, Pushkar and Aniruddha for their support in general and lessons of life. Finally, I would love to thank all the authors in the bibliography, all my professors, staffs in LSU and Temple Universities for their knowledge, wisdom and help.

TABLE OF CONTENTS

LIST OF FIGURES

Figure

LIST OF TABLES

Table

CHAPTER 1

THEORY

1.1 Density Functional Theory

The term density functional theory (DFT) refers to all methods that express the ground-state energy as a functional of the electronic density $n(\mathbf{r})$. Within DFT, the total energy of a system is a functional of density $n(\mathbf{r})$. Finding out the total energy of a system with the help of electron density and writing energy as a functional of electron density started early.

1.1.1 Thomas and Fermi Model

In 1927, Thomas and Fermi independently employed the electron density rather than wave function to compute the total energy of many-body system. In Thomas-Fermi density functional, the energy functional, which has been drived from the uniform electron gas, is given by

$$E[n] = \frac{3}{10}(3\pi^2)^{2/3}\int d\mathbf{r}[n(\mathbf{r})]^{5/3} + \frac{1}{2}\int d\mathbf{r}\int d\mathbf{r}^{,}\frac{n(\mathbf{r})n(\mathbf{r}^{,})}{\mathbf{r}-\mathbf{r}^{,}} + \int d\mathbf{r}v(\mathbf{r})n(\mathbf{r}) \quad (1.1\text{-}1)$$

where, the first term on the right hand side of (1.1-1) gives the kinetic energy for the given electron density distribution, the second term is the classic Coulomb interaction between two electron density distributions and the third term is the interaction with the external potential $v(\mathbf{r})$. It has been shown that the Thomas-Fermi energy functional can give reasonable results for heavy atoms; however, it is not accurate for molecules and solids. The molecules in Thomas-Fermi theory are un-

bound, because the exchange-correlation energy, which is responsible for most of the cohesive energy in condensed phases, is completely ignored in this energy functional. Later, the exchange-correlation effects were included in several other earlier versions of density functionals such as Thomas-Fermi-Dirac approximation (with local exchange only), Thomas-Fermi-Dirac-Gombas approximation (local exchange-correlation) and Thomas-Fermi-Dirac-Gombas-Weizscker (semilocal correction to kinetic energy and local exchange-correlation). Those earlier energy functionals are considered to be still very rough approximations for molecules and solids. They do not predict very accurate cohesive energies and equilibrium geometries for condensed phases. Therefore, they have never been widely used in any practical calculations for condensed phases.

1.1.2 Hohenberg and Kohn Theorem

After Thomas and Fermi, Hohenberg and Kohn introduced the energy functional as,

$$E[n] := F[n] + \int d\mathbf{r} n(\mathbf{r}) v(\mathbf{r})$$
$$F[n] := \min_{\Psi \to n} \langle \Psi | \hat{T} + \hat{V}_{ee} | \Psi \rangle \qquad (1.1\text{-}2)$$

and proved that,

1. F[n] is a unique functional of the density n($\mathbf{r}$) i.e., for an N electron system, there do not exist two ground state wavefunctions $\Psi_1 \neq \Psi_2$ (potentials $v_1 \neq v_2$) resulting in the same density n($\mathbf{r}$).[*Hohenberg and Kohn*, 1964]

2. The energy functional E obeys a variational principle and always results in energies larger or equal to the ground state energy E_g such that,$E[n] \geq E_g$ and it reaches the ground-state energy at the ground-state density so that, $E[n_g] = E_g$.

For the N electron system, minimizing (1.1-2) by varying the many-body wavefunction in 3N space is almost a formidable task. Using the Levy-Leib constrained search, the problem of optimizing the wavefunction has been transformed into the minimization of $E[n]$ by trial electron density n($\mathbf{r}$) in 3-dimensional space. However, using Levy's method within density functional theory framework is still not practical. Although the Hohenberg-Kohn (HK) theorem provides a theoretical justification for the construction of an energy functional that depends on the electron density only, it does not provide a concrete expression for the energy functional F[n].

1.1.3 Kohn and Sham Theorem

Later in 1965, Kohn and Sham proposed a different approximation for the functional F[n] that maps the problem of a system of interacting particles onto a system of independent electrons with the same density n($\mathbf{r}$) moving in an effective local potential that mimics the influence of the other electrons.[*Kohn and Sham*, 1965] The form of the universal density functional is given by,

$$F[n] = T_s[n] + E_H[n] + E_{xc}[n] \tag{1.1-3}$$

and the energy of an electron system can be then reformulated to,

$$E[n] = F[n] + \int n(\mathbf{r}) v_{ext}(\mathbf{r}) d\mathbf{r}$$

$$E[n] = T_s[n] + E_H[n] + E_{xc}[n] + E_{ext}[n] \tag{1.1-4}$$

In this equation, the kinetic energy density functional is represented by $T_s[n]$, and $E_H[n]$ is the classical electrostatic energy (Hartree energy) of the non-interacting electrons. $E_{xc}[n]$ refers to the exchange-correlation energy, mainly accounting for the missing many-body effects in the Kohn-Sham system. $E_{ext}[n]$ is the energy corresponding to the external potential. In equation (1.1-2) $F[n]$ is derived from the

wavefunction of the true, interacting, system which is thereby denoted as Ψ, whereas in the equation (1.1-3) $T_s[n]$ is derived from the wavefunction of the reference system of independent particles is a Slater determinant built from one-electron single particle Kohn-Sham orbital wavefunctions $\{\psi_i\}$. The independent particle kinetic energy $T_s[n] = \hbar^2/2m \sum_{i(occ)} \langle\psi_i| \nabla^2 |\psi_i\rangle$ thereby depends only implicitly on the electron density $n(\mathbf{r}) = \sum_i f_i|\psi_i(\mathbf{r})|^2$ via the one-electron wavefunctions $\{\psi_i\}$, where f_i is the Fermi-Dirac distribution function for the $i-th$ Kohn-Sham single particle orbital. The Hartree potential is $v_H = \int \frac{n(\mathbf{r}')}{|\mathbf{r}-\mathbf{r}'|} d\mathbf{r}'$ and the exchange-correlation potential density is $v_{xc} = \frac{\delta E_{xc}}{\delta n}$. Then from the equation (1.1-4) energy we get,

$$E[n] = T_s[n] + \int n(\mathbf{r})[\frac{1}{2} v_H[n](\mathbf{r}) + v_{ext}(\mathbf{r})] d\mathbf{r} + E_{xc}[n]$$
$$E_{KS}[n] = T_s[n] + \int n(\mathbf{r}) v_{KS}[n](\mathbf{r}) d\mathbf{r} \qquad (1.1\text{-}5)$$

Since by assumption the interacting and non-interacting systems have the same ground state density $n(\mathbf{r})$, they also have same Euler equation, $\frac{\delta E}{\delta n(\mathbf{r})} = \mu$ and $\frac{\delta E_{KS}}{\delta n(\mathbf{r})} = \mu$ respectively. Hence, the ground state energy can be obtained by minimizing this energy with respect to the density and solving the corresponding Kohn-Sham equations given by,

$$(\frac{-\hbar^2}{2m}\nabla^2 + v_H[n](\mathbf{r}) + v_{xc}[n](\mathbf{r}) + v_{ext}[n](\mathbf{r}))\psi_i = \epsilon_i \psi_i$$
$$(\frac{-\hbar^2}{2m}\nabla^2 + v_{KS}[n](\mathbf{r}))\psi_i = \epsilon_i \psi_i$$
$$, \qquad (1.1\text{-}6)$$

where $v_{xc}[n](\mathbf{r}) = \frac{\delta E_{xc}}{\delta n(\mathbf{r})}$. Obviously, ϵ_i denotes the eigen-energy corresponding to the ith Kohn-Sham single particle orbital. Meanwhile, the effective potential of Kohn-Sham theory is described as, $v_{KS} = v_{eff} = v_H + v_{xc} + v_{ext}$ and is definitely a function of density n($\mathbf{r}$) such that the above Kohn-Sham equations can be rewritten as a simple

Schrodinger-like equation $(\frac{-\hbar^2}{2m}\nabla^2 + v_{eff}[n](\mathbf{r}))\psi_i = \epsilon_i\psi_i$.

1.1.3.1 Adiabatic Connection

The fully-interacting Hamiltonian can be described by a coupling constant(λ) as H_λ,

$$H_\lambda = T + V_\lambda + \lambda V_{ee} \tag{1.1-7}$$

Here, the value of coupling constant λ defines the strength of an effective interaction between electrons as λV_{ee} where V_{ee} is Coulomb interaction. Similarly, H_λ also contains a coupling constant dependent single particle potential V_λ as well so that $V_\lambda = \sum_i v_\lambda(\mathbf{r}_i)$, where the local potential $v_\lambda(\mathbf{r}_i)$ is adjusted in such a way that the ground state solution of H_λ has exactly the same electron density as that of the ground state solution of the fully interacting ($\lambda = 1$) Hamiltonian in any path connecting λ from 0 to 1. $V_1 = \sum_i v_{ext}(\mathbf{r}_i)$ and $V_0 = \sum_i v_{KS}(\mathbf{r}_i)$. Hence at $\lambda = 0$, H_λ represents the Kohn-Sham(KS) Hamiltonian. The interacting kinetic energy T is replaced by non interacting KS kinetic energy T_s and the difference is taken care of in the KS exchange-correlation energy. The fixed-density path connecting $\lambda = 0$ and $\lambda = 1$ is known as the adiabatic connection. Note that, with the help of the adiabatic connection, H_0 can describe a system of non-interacting electrons (Kohn-Sham system) with a fully-interacting density at the ground state. Hence, the total energy functional of an interacting system is successfully represented by a system with non-interacting electrons moving in the effective external potential (v_{eff}), described in the previous section. We will elaborate the perks of adiabatic connections more while describing the ACFD (Adiabatic Connection Fluctuation Dissipation) Theory framework later on.

1.2 Exchange-Correlation Functional

From the adiabatic connection of the previous section we conclude that for $\lambda = 1$,

$$E[n] = T[n] + E_{ext}[n] + E_{ee}[n] \tag{1.2-8}$$

whereas for $\lambda = 0$,

$$E[n] = T_s[n] + E_{eff}[n] = T_s[n] + E_H[n] + E_{xc}[n] + E_{ext}[n]. \tag{1.2-9}$$

Therefore, the exchange-correlation energy functional can be given by $E_{xc}[n] = T[n] - T_s[n] + E_{ee}[n] - E_H[n]$, i.e. by simply the sum of the error made in using a non-interacting kinetic energy and the error made in treating the electron-electron interaction classically. $E_{xc}[n]$ practically can be evaluated according to the Jacob's ladder of the density functional framework proposed by Perdew-Schmidt[*Perdew et al.*, 2001].

The first rung is the simplest Local Density Approximation (LDA) where the exchange-correlation energy density at each point in space is the same as that for an uniform electron gas with the electron density for that point. The exchange-correlation functional is only dependent on n($\mathbf{r}$) and given by,

$$E_{xc}[n] = \int n(\mathbf{r}) {\epsilon_{xc}}^{LDA}(n(\mathbf{r}))d\mathbf{r} = \int n(\mathbf{r}) {\epsilon_{xc}}^{unif}(n(\mathbf{r}))d\mathbf{r}. \tag{1.2-10}$$

Here, ${\epsilon_{xc}}^{unif}(n(\mathbf{r}))$ represents the exchange-correlation density functional of the uniform electron gas. Although, the exchange energy density functional in the uniform limit can be determined analytically, the correlation energy density is only known numerically through quantum Monte Carlo calculations. Hence different parameterizations give rise to the different versions of LDA density functional (${\epsilon_{xc}}^{LDA}(n(\mathbf{r}))$).

The second rung is a natural extension beyond LDA, where constructing the

exchange-correlation density functional, gradient of density ($\nabla n(\mathbf{r})$) is also considered an argument alongside of density ($n(\mathbf{r})$). This is known as the Generalized Gradient Approximation (GGA). In this case, the exchange-correlation functional is dependent on the electron density $n(\mathbf{r})$ and the gradient of electron density around that point. The exchange-correlation functional is given by,

$$E_{xc}[n] = \int n(\mathbf{r}) {\epsilon_{xc}}^{GGA}(n(\mathbf{r}), \nabla n(\mathbf{r}))d\mathbf{r}. \tag{1.2-11}$$

GGA functionals can be either non-empirical or empirical, based on their constructions. Non-empirical GGA functionals are constructed to fulfill some exact conditions whereas, empirical GGA functionals are constructed by fitting to the energies calculated by a higher level of theory or experimental values.

The third rung is the meta-GGA, where constructing the exchange-correlation density functional, either the Laplacians $\nabla^2 n(\mathbf{r})$ of density or the kinetic energy density $\tau(\mathbf{r})$ are added to the arguments alongside of the gradient of density and density. So the exchange-correlation functional within the meta-GGA approximation is given by,

$$\begin{aligned} E_{xc}[n] &= \int n(\mathbf{r}) {\epsilon_{xc}}^{GGA}(n(\mathbf{r}), \nabla n(\mathbf{r}), \nabla^2 n(\mathbf{r}))d\mathbf{r} \\ or E_{xc}[n] &= \int n(\mathbf{r}) {\epsilon_{xc}}^{GGA}(n(\mathbf{r}), \nabla n(\mathbf{r}), \tau(\mathbf{r}))d\mathbf{r}. \end{aligned} \tag{1.2-12}$$

The kinetic energy density is, $\tau(\mathbf{r}) = \frac{1}{2}\sum_i^{occupied} |\nabla \psi_i(\mathbf{r})|^2$ where the KS orbital wavefunctions $\psi_i(\mathbf{r})$ are implicit functionals of density. In the limit of slowly varying density the kinetic energy density contains the same information as the Laplacians of the density. Because of this and the ability to fit more physical constraints, the explicit dependence on the Laplacian of the density is mostly neglected while constructing meta-GGAs in practice.

The fourth rung is the hyper-GGA or hyper-meta-GGA level, where for obtaining the exchange-correlation density functional, some part of semilocal exchange-correlation energy of the first three rungs is mixed with the some part of Hartree-Fock like exact exchange which is non-local in space and dependent on the occupied KS orbital wavefunctions (ψ_i) in general. These functionals are also called hybrid functionals. Almost all the hyper-GGAs or hyper-meta-GGAs have non-local exchange but semilocal correlations. Even though, the inclusion of the Hartree-Fock like exact exchange does allow for more empirical parameters to be satisfied, but it has been argued that a so-called hyper-GGA or hyper-meta-GGA must contain at least one empirical parameter in its construction resulting in the non zero possibility of problems of non-transferability for even the best possible hyper-GGA or hyper-meta-GGA across all the systems.

The fifth and highest rung is called Random Phase Approximations (RPA) where both occupied and unoccupied KS orbital wavefunctions are used in order to find the exchange-correlation density functional. Both exchange and correlation are non-local. For the exchange part, the full Hartree-Fock-like exact exchange is used. For a non-local construction of correlation, RPA can effortlessly describe the long range dispersion interactions.

The computational complexity is typically increased with the higher rung and accuracy is also normally increased as well.

1.2.1 LDA

Some of the most popular LDA functionals are the Ceperley-Alder (CA)[*Ceperley and Alder*, 1980], Perdew-Zunger (PZ)[*Perdew and Zunger*, 1981b] and Vosko-Wilk-Nusair (VWN)[*Vosko et al.*, 1980] approximations. The exchange part has the common analytic form, ${\epsilon_x}^{LDA} = {\epsilon_x}^{unif} = -\frac{3}{4\pi}(3\pi^2 n)^{1/3} = -\frac{0.458}{r_s}$ where r_s is the Wigner-Seitz radius of the uniform electron gas given by, $r_s = \frac{3}{4\pi n^{1/3}}$. Ceperley-Alder has

found the total energy of uniform electron gas for different r_s values using Green's Function Monte Carlo simulation, and then found the parametrized form of the correlation part as, ${\epsilon_c}^{LDA} = {\epsilon_c}^{unif} = \frac{A}{(1+B{r_s}^{1/2}+Cr_s)}$ for $r_s \geq 1$ in the non-spin-polarized case, where A = -0.1423, B = 1.0529, C = 0.334. Similarly, Perdew-Zunger has provided the parametrized form of the correlation part in the non-spin-polarized case as, ${\epsilon_c}^{LDA} = {\epsilon_c}^{unif} = A \ln r_s + B + Cr_s \ln r_s + Dr_s$ for $r_s \leq 1$ where A = 0.0311, B = -0.048, C = 0.0020, D = -0.0116 and ${\epsilon_c}^{LDA} = {\epsilon_c}^{unif} = \frac{A}{(1+B{r_s}^{1/2}+Cr_s)}$ for $r_s > 1$ where A = -0.1423, B = 1.0529, C = 0.334. In the $r_s \leq 1$ dense electron systems, the random phase approximation (RPA) provides the parameter A for this LDA.

The electron densities in molecules and solids are far from uniform and even have cusps at the nuclei. The density is so far from being uniform or homogeneous that the use of the LDA was greeted initially by great reserve, particularly in the world of chemistry. But LDA almost always leads to the correct picture of binding trend across and down the periodic table. Structures, bond lengths, and vibration frequencies in many systems are reproduced satisfactorily, and the deviations from measurements of these and other quantities are often quite systematic.Lattice constants in solids are usually underestimated. Binding energies of molecules and cohesive energies of solids are usually overestimated. In weakly bound systems, e.g., where closed-shell molecules bind, these overestimations are often large, and the bond lengths are too short. In finite systems (atoms, surfaces) the exchange-correlation potential decays exponentially rather than with the inverse power of distance. This is one of the consequences of the incomplete self-interaction correction. Negative ions are often unbound, although it may be possible to estimate binding energies in some cases. In semiconductors the energy gap between valence and conduction bands is much less than the measured values. The so-called strongly correlated systems, such as the insulating 3d-transition metal oxides, are not described well by LDA calculations, which often predict them to be metallic.

1.2.2 GGA

The earlier Gradient Expansion Approximation (GEA) of exchange-correlation energy has the form for the non-spin-polarized case as,

$$E_{xc}{}^{GEA}[n] = E_{xc}{}^{LDA}[n] + \int C_{xc}(n)\frac{|\nabla n(\mathbf{r})|^2}{n^{4/3}(\mathbf{r})}d\mathbf{r} \qquad (1.2\text{-}13)$$

where $C_{xc}(n)$ is a derived coefficient. The GGA form is asymptotically valid for slowly varying densities and definitely an improvement over LDA in that limit by including some inhomogeniety of neighboring densities at point r. The straightforward evaluation of this expansion proved to be illbehaved because this is not monotonically convergent and singularities arising in the process only cancel out if infinite terms are summed up. The largest error comes from the correlation part which was later fixed by a wave-vector space cutoff method of Langreth and Mehl[*Langreth and Mehl*, 1981]. Further studies proved that the gradient expansion should be carried out carefully in order to retain all contributions from the desired order and one needs to be careful about satisfying some exact conditions for the exchange and correlation hole while as well, such as, the normalization condition, negativity of exchange density and so on. Eventually a number of modified gradient expansion approximations came out mainly aiming to satisfy those exact conditions by Perdew et al. and they became known as Generalized Gradient Approximations (GGA). The non-empirical GGA exchange part can be given by the general form of the non-spin-polarized case as, $E_x{}^{GGA} = \int n(\mathbf{r})\epsilon_x{}^{unif}(n(\mathbf{r}))F_x(s)d\mathbf{r}$ where $F_x(s)$ is known as the gradient enhancement factor of exchange and s symbolizes the dimensionless reduced density gradient as, $s = |\nabla n(\mathbf{r})|/(2k_F n(\mathbf{r}))$ where k_F is Fermi wave vector given by, $k_F = (3\pi^2 n)^{1/3}$. Now depending on the different $F_x(s)$ functional form with value of different parameters along with their capability of satisfying as many exact conditions, different GGA functionals are created. Among them, the Perdew-

Burke-Erzenhoff (PBE)[*Perdew et al.*, 1996b] is the most popular one. For, PBE $F_x(s) = 1 + \kappa - \frac{\kappa}{1+\mu s^2/\kappa}$ where $\kappa = 0.804$ and $\mu = 0.21951$. Similarly, for the correlation the form is, ${E_c}^{GGA} = \int n(\mathbf{r}){\epsilon_c}^{unif}(n(\mathbf{r}))H(n(\mathbf{r}),t)d\mathbf{r}$ where $H(n(\mathbf{r}),t)$ is the gradient correction to the correlation and t is also a dimensionless density gradient given by $t = |\nabla n(\mathbf{r})|/(2k_s n(\mathbf{r}))$ where k_s is local Thomas-Fermi screening wave-vector given by $k_s = \sqrt{4k_F/a_0\pi}$ where a_0 denotes Bohr radius. Similar to the exchange case, for different functionals $H(n(\mathbf{r}),t)$ has different functional forms as well as different values of parameters. For PBE, $H(n(\mathbf{r}),t) = \gamma \ln(1 + \frac{\beta}{\gamma}t^2[\frac{t^2+At^4}{1+At^2+A^2t^4}])$ for non-spin-polarized case. Now, $A = \frac{\beta}{\gamma}[e^{\frac{-{\epsilon_c}^{unif}(n)}{\gamma}} - 1]^{-1}$, $\beta = 0.066725$ and $\gamma = 0.031091$. There are some GGA functionals such as, BLYP, which fit gradient expansion expression parameters of their functional forms of exchange and correlation to experimental molecular data. They do not satisfy the exact conditions and hence work well for molecules, but face problems for solids due to transferability issues.

In comparison to LDA, GGAs usually improve the binding energies, atomic energies, bond lengths and angles. They improve the energetics, geometry and dynamical properties of water, ice, water clusters etc. They also give a better description of the systems with hydrogen bonds. Normally they slightly improve the band gap but overestimate the lattice constants in general. For noble metals, LDA gives much better lattice constants than GGA compared to the experimental results, mostly due to the fortuitous error cancellations of the exchange and correlation holes. PBE has the same problem of exponential decay of exchange-correlation potential,as LDA has away from atoms instead of the (-1/r) behavior. GGAs don't either improve LDA results much for strongly correlated systems, with partially filled d and f shells. The energy and geometry dilemma is an important aspect for semilocal functionals. GGA gives wrong energetics while giving very good geometry i.e. lattice constants and vice versa. That's why more ingredients are needed in exchange-correlation functionals beyond GGA.

1.2.3 meta-GGA

The meta-GGAs that depend upon the kinetic energy density $\tau(\mathbf{r})$ to quantify the one or two electron region differ from the meta-GGAs that depend instead on the laplacian of the density known as meta-GGA-Ls[*Mejia-Rodriguez and Trickey*, 2017]. Perdew-Kurth-Zupan-Blaha (PKZB),[*Perdew et al.*, 1999] Tao-Perdew-Staroverov-Scuseria (TPSS)[*Tao et al.*, 2003] and the recent SCAN[*Sun et al.*, 2015] belong to the first type whereas Zhao-Truhlar's M06 family of meta-GGAs[*Zhao and Truhlar*, 2008] is a mixture of the two types. The important dimensionless ratios that involve the kinetic energy density which appear in the meta-GGA context are, $z[n], \alpha[n]$ and $w[n]$ given by,

$$z[n] = \frac{\tau_W[n]}{\tau[n]}, \alpha[n] = \frac{\tau[n] - \tau_W[n]}{\tau_{TF}}, w[n] = \frac{\tau_{TF}[n]/\tau_W[n] - 1}{\tau_{TF}[n]/\tau_W[n] + 1} \tag{1.2-14}$$

where τ_{TF} is Thomas Fermi kinetic energy density or kinetic energy density of uniform electron gas given by, $\tau_{TF} = \frac{3}{10}(3\pi^2)^{2/3} n^{5/3}(\mathbf{r})$ and τ_W is von Weizsacker kinetic energy density given by, $\tau_W = \frac{5}{3}\tau_{TF} s^2$ where s is the reduced density gradient as given earlier by $s = |\nabla n(\mathbf{r})|/(2(3\pi^2)^{1/3} n^{4/3}(\mathbf{r}))$. Note that w[n] has become very popular in the development of semiempirical meta-GGAs of Becke and others, while z[n] was used in early non-empirical meta-GGAs such as PKZB, TPSS. Recently $\alpha[n]$ was used in meta-GGA "made very simple" (MVS) and SCAN of Perdew and co-workers. The exchange part can be given for the non-spin-polarized case by ${E_x}^{meta-GGA} = \int n(\mathbf{r}) {\epsilon_x}^{unif}(n(\mathbf{r})) F_x(s,\tau) d\mathbf{r}$ where the exchange enhancement factor F_x depends on s,α or s,z or s,w in various functionals with different functional forms and different values of parameters.

For SCAN, we have $F_x(s,\alpha) = ({h_x}^1(s,\alpha) + f_x(\alpha)[1.174 - {h_x}^1(s,\alpha)])g_x(s)$ where ${h_x}^1(s,\alpha) = 1 + \frac{k_1 x}{k_1 + x}$ where $k_1 = 0.065$ and $x = \mu_{GE} s^2 [1 + \frac{b_4 s^2}{\mu_{GE}} e^{-\frac{b_4 s^2}{\mu_{GE}}}] + [b_1 s^2 + b_2(1-\alpha)e^{-b_3(1\alpha)}]^2$ where $\mu_{GE} = 10/81 = 0.12345679$, $b_1 = (511/13500)/(2b_2)$, $b_2 =$

$\sqrt{5913/405000}$, $b_3 = 0.5$, $b_4 = {\mu_{GE}}^2/k_1 1606/18225{b_1}^2$. $g_x(s) = 1 - e^{-a_1/\sqrt{s}}$ where $a_1 = 4.9479$. Then $f_x(\alpha) = e^{-c_{1x}\alpha/(1-\alpha)}\theta(1-\alpha) - d_x e^{c_{2x}/(1-\alpha)}\theta(\alpha-1)$ where $\theta(y)$ is a step function of y, $c_{1x} = 0.667$, $c_{2x} = 0.8$, $d_x = 1.24$. So for the exchange part SCAN gives ${E_x}^{SCAN} = \int n(\mathbf{r}){\epsilon_x}^{unif}(n(\mathbf{r}))F_x(s,\alpha)d\mathbf{r}$.

For the SCAN correlation part, ${E_c}^{SCAN} = \int n(\mathbf{r})[{\epsilon_c}^{revPBE}(\alpha=0) + f_c(\alpha)[{\epsilon_c}^{revPBE}(\alpha = 0) - {\epsilon_c}^{revPBE}(\alpha=1)]]d\mathbf{r}$ where $f_c(\alpha) = e^{-c_{1c}\alpha/(1-\alpha)}\theta(1-\alpha) - d_c e^{c_{2c}/(1-\alpha)}\theta(\alpha-1)$ where $\theta(y)$ is a step function of y, $c_{1c} = 0.64$, $c_{2c} = 1.5$, $d_x = 0.7$. SCAN can capture covalent bonds ($\alpha = 0$), metallic bonds ($\alpha = 1$) and weak bonds ($\alpha >> 1$) because of its construction.

The meta-GGAs, especially SCAN, give both accurate energetics and accurate geometry simultaneously. Also it can capture intermediate van der Waals interaction and hence gives better binding energies in weakly bound systems and molecular systems compared to LDA and GGA.

1.3 Dispersion Corrections

Dispersion interactions arise from induced dipole - induced dipole attractive interactions owing to charge fluctuations in the atoms or molecules or in parts of any extended system. It has a long range (C_6/R^6) behavior where R is the distance between the molecules or atoms. C_6 is known as London coefficient. $R = |\mathbf{r} - \mathbf{r}'|$ is non-local in space. Close to the atoms the van der Waals interactions can be described by semilocal correlations and corresponding localized exchange and correlation holes. But for long-range it needs either empirical atom pairwise correlation dispersion corrections of DFT+D families of Grimme et al.[*Grimme et al.*, 2010] or Tkatchenko-Scheffler (TS)[*Tkatchenko and Scheffler*, 2009] methods or semi empirical electron density based non-local correlation kernel dispersion corrections of vdW-DF families of the Rutgers-Chalmers group[*Dion et al.*, 2004; *Klimeš et al.*, 2011] and VV10 families of Vydrov-van Voorhis[*Sabatini et al.*, 2013; *Vydrov and Van Voorhis*, 2009]. In the first

type of methods, pairwise interatomic terms are added to the DFT potentials, with explicit usage of C_6 parameters and a damping function. In the second type of methods, the missing dispersion is provided by adding a non-local correlation component to semilocal exchange-correlation energy such that $E_{xc} = {E_{xc}}^{semilocal} + {E_c}^{nl}$, where E_{xc} is the total exchange-correlation energy.

The revised VV10 (rVV10) approximation is parametrized using only the local density and its reduced gradient. Two free empirical parameters are needed to determine the model, C and b. First (C) is adjusted to reproduce reference dispersion coefficients at large distances at the asymptotic limit, and second (b) is used to damp the rVV10 contribution at short distances. The parameter b can be used to adjust the rVV10 functional to any semilocal Density Functional Approximation (DFA) while C is kept at its original value while mixing the non-local ${E_c}^{nl}$ with the semilocal exchange-correlation. Mixing with SCAN, the optimized value of C =0.0093 and b = 15.7.[*Peng et al.*, 2016]

The damping functions are introduced to combine the D3 dispersion interaction with the semilocal correlation contribution from the DFA. The two-body damping can be used either with a zero damping (one free parameter rs_6) or a rational (Becke-Johnson) damping (two free parameters a_1 and a_2). The dipole-quadrupole C_8 terms can be scaled by a parameter s_8, which improves the interpolation between various DFAs with substantially different behavior in the intermediate correlation regime. For SCAN, the optimized value of $a_1 = 0.538$ and $a_2 = 5.42$.[*Brandenburg et al.*, 2016a] D3 also includes some three-body interactions in the formulation.

1.4 ACFD Theory

From the adiabatic connection and Hellmann-Feynman theorem, the total exchange-correlation energy $E_{Hxc} = E_H + E_{xc}$ can be found by integrating between the KS system at $\lambda = 0$ and the fully interacting system at $\lambda = 1$ as, $E_{Hxc} = E_{lambda=1} - E_{\lambda=0} =$

$\int_0^1 \frac{d}{d\lambda} < \psi_\lambda|\hat{H(\lambda)}|\psi_\lambda > d\lambda = \int_0^1 < \psi_\lambda|\frac{d\hat{H(\lambda)}}{d\lambda}|\psi_\lambda > d\lambda$. From this one can easily derive that, $E_{Hxc} = \int_0^1 < \psi_\lambda|\hat{V_{ee}}|\psi_\lambda > d\lambda$ where $\hat{V_{ee}}$ is the Coulomb interaction operator. The expectation value of the Coulomb operator can be written by using the pair density as, $< \psi_\lambda|V_{ee}|\psi_\lambda >= \frac{e^2}{2}\int \frac{n^{2,\lambda}(\mathbf{r},\mathbf{r'})}{|\mathbf{r}-\mathbf{r'}|}d\mathbf{r}d\mathbf{r'}$. After expressing the pair density through the density operator $\hat{n}(\mathbf{r}) = \sum_i \delta(\mathbf{r}-\mathbf{r}_i)$ one can derive E_{Hxc} via fluctuation dissipation theorem which states that, the density-density response function χ of a system with a small time-dependent perturbative potential can be described by the linear density response properties of the system in the same manner as its response to a spontaneous density fluctuation, as

$$E_{Hxc} = \frac{e^2}{2}\int_0^1 d\lambda \int \frac{1}{|\mathbf{r}-\mathbf{r'}|}[n(\mathbf{r})n(\mathbf{r'}) - (\frac{1}{\pi}\int_0^\infty \chi^\lambda(\mathbf{r},\mathbf{r'},i\omega)d\omega) - n(\mathbf{r})\delta(\mathbf{r}-\mathbf{r'})]d\mathbf{r}d\mathbf{r'} \tag{1.4-15}$$

The first term is clearly the Hartree term and two other terms constitute the exchange-correlation part. After further simplications one can get,

$$E_{xc} = E_x[\psi_{KS}] + E_c \tag{1.4-16}$$

where first one is the exact exchange and the second one is the correlation given by

$$E_c = -\int_0^1 d\lambda \int \frac{e^2}{|\mathbf{r}-\mathbf{r'}|}(\int_0^\infty [\chi^\lambda(\mathbf{r},\mathbf{r'},i\omega) - \chi^{KS}(\mathbf{r},\mathbf{r'},i\omega)]\frac{d\omega}{2\pi})d\mathbf{r}d\mathbf{r'} \tag{1.4-17}$$

Here $\frac{e^2}{|\mathbf{r}-\mathbf{r'}|} = V(\mathbf{r},\mathbf{r'})$ is the bare Coulomb interaction. From the Dyson-type equation we can express χ^λ as,

$$\chi^\lambda(\mathbf{r},\mathbf{r'},i\omega) = \chi^{KS}(\mathbf{r},\mathbf{r'},i\omega) + \int \chi^{KS}(\mathbf{r},\mathbf{r}_1,i\omega)[V^\lambda(\mathbf{r}_1,\mathbf{r}_2) + {f_{xc}}^\lambda(\mathbf{r}_1,\mathbf{r}_2,i\omega)]\chi^\lambda(\mathbf{r}_2,\mathbf{r'},i\omega)d\mathbf{r}_1 d\mathbf{r}_2 \tag{1.4-18}$$

$f_{xc}(\mathbf{r}_1, \mathbf{r}_2, i\omega)$ is the exact frequency dependent exchange-correlation kernel. The scaled Coulomb interaction is linear in the coupling strength, $V^\lambda = \lambda V$. The behavior of the xc-kernel can be determined from uniform coordinate scaling, though we focus here on kernels which scale linearly with coupling strength λ. Once the kernel and the KS response function are available, the interacting response function can be extracted by solving the Dyson-type equation and the correlation energy computed from the Eq. 1.4-17. We will call a direct solution of the Dyson-type equation and the corresponding correlation energy including the xc kernel as the infinite-order method in this chapter, since by inversion

$$\chi^\lambda(i\omega) = ((\chi^{KS}(i\omega))^{-1} - V^\lambda - {f_{xc}}^\lambda(i\omega))^{-1}. \tag{1.4-19}$$

Since f_{xc} appears in the inverse it has been included in the response-function, and consequently in the correlation energy, through infinite-order in the traditional many-body perturbation theory sense. For the simplest ACFD-based method RPA, the kernel part i.e. $f_{xc}^\lambda = 0$.

1.4.1 RPA renormalization

RPA renormalization (RPAr) is an alternative formulation of many-body perturbation theory that naturally includes screening effects in beyond RPA (bRPA) correlation through its dependence on the RPA response function. By a slight rearrangement in Eq. 1.4-19, the Dyson-type equation can be expressed as,

$$\chi^\lambda(i\omega) = \hat{\chi}^\lambda(i\omega) + \hat{\chi}^\lambda(i\omega){f_{xc}}^\lambda(i\omega)\chi^\lambda(i\omega) \tag{1.4-20}$$

where the RPA response function is $\hat{\chi}^\lambda(i\omega) = ((\chi^{KS}(i\omega))^{-1} - V)^{-1} = (1 - \chi^{KS}(i\omega)V)^{-1}\chi^{KS}(i\omega)$. If the xc kernel is kept to infinite-order in Eq. 1.4-20, the resulting correlation energy is equivalent to that from the infinite-order approach. The utility of RPAr there-

fore lies in approximations to Eq. 1.4-20, which we can obtain order-by-order just by expanding the inverse in powers of the product $\hat{\chi}^{\lambda}(i\omega){f_{xc}}^{\lambda}(i\omega)$ elaborated below as,

$$\begin{aligned}\chi^{\lambda}(i\omega) &= (1-\hat{\chi}^{\lambda}(i\omega){f_{xc}}^{\lambda}(i\omega))^{-1}\hat{\chi}^{\lambda}(i\omega) \\ &\approx \hat{\chi}^{\lambda}(i\omega)+\hat{\chi}^{\lambda}(i\omega){f_{xc}}^{\lambda}(i\omega)\hat{\chi}^{\lambda}(i\omega)+\hat{\chi}^{\lambda}(i\omega){f_{xc}}^{\lambda}(i\omega)\hat{\chi}^{\lambda}(i\omega){f_{xc}}^{\lambda}(i\omega)\hat{\chi}^{\lambda}(i\omega)+.....\end{aligned} \tag{1.4-21}$$

The correlation energy is then obtained as a sum of the RPA correlation energy, which is zeroth-order in RPAr, and all bRPA contributions as given by $E_c[f_{xc}] = {E_c}^{RPA} + \sum_{n=1}^{\infty}{\Delta E_c}^{RPArn}[f_{xc}]$ where the n-th order RPAr correction for a given kernel is

$${\Delta E_c}^{RPArn}[f_{xc}] = -\int_0^1 d\lambda \int_0^{\infty} < V(\hat{\chi}^{\lambda}(i\omega){f_{xc}}^{\lambda}(i\omega))^n \hat{\chi}^{\lambda}(i\omega) > \frac{d\omega}{2\pi} \tag{1.4-22}$$

and the total infinite-order bRPA correction can be computed as,

$$\begin{aligned}{\Delta E_c}^{bRPA} &= E_c[f_{xc}] - {E_c}^{RPA} \\ &= -\int_0^1 d\lambda \int_0^{\infty} < V(\hat{\chi}^{\lambda}(i\omega){f_{xc}}^{\lambda}(i\omega))\chi^{\lambda}(i\omega) > \frac{d\omega}{2\pi}\end{aligned} \tag{1.4-23}$$

In keeping with our previous naming conventions, when a given kernel is referenced directly as a correlation method in this chapter we mean the infinite-order method, Eq. 1.4-24. The acronym XACFD is also used to mean the exact ACFD correlation (infinite order) with a given kernel. For exchange-like kernels an analytic integral exists for the first-order (RPAr1) correction. RPAr1 also guarantees the elimination of divergences due to electronic instabilities. Compared to the infinite-order method, RPAr1 systematically underestimates the bRPA correction by approximately 10%, which can be straightforwardly accounted for through the inclusion of higher-order terms in the RPAr series.

1.4.2 Higher Order Terms (HOT) Approximation

The drawback of higher-orders in the RPAr series is that an analytic coupling-strength integral is not currently known for those terms and thus a numerical coupling-strength integration must be reintroduced just to compute a small fraction of the energy. In order to bypass the coupling-strength integration entirely, we have developed a higher- order terms (HOT) approximation that seeks to account for the missing correlation beyond RPAr1.

We have studied the coupling-strength dependence of the integrands in Eq. 1.4-22 and found that an accurate approximation can be obtained from a second-order correction to the response function. We start with the exact definition of correlation beyond RPAr1,

$$\begin{aligned}\Delta E_c{}^{bRPAr1} &= E_c[f_{xc}]^{bRPA} - E_c[f_{xc}]^{RPAr1} \\ &= -\int_0^1 d\lambda \int_0^\infty < V(\hat{\chi}^\lambda(i\omega) f_{xc}{}^\lambda(i\omega)\hat{\chi}^\lambda(i\omega) f_{xc}{}^\lambda(i\omega))\chi^\lambda(i\omega) > \frac{d\omega}{2\pi}\end{aligned} \tag{1.4-24}$$

We decompose this correlation energy into kinetic(T_c) and potential(U_c) contributions and write the total correction in terms of the potential contribution as,

$$\Delta E_c[f_{xc}]^{bRPAr1} = (1-\hat{b})\Delta U_c[f_{xc}]^{bRPAr1}, \hat{b} = -\frac{\Delta T_c{}^{bRPA} - \Delta T_c{}^{RPAr1}}{\Delta U_c{}^{bRPA} - \Delta U_c{}^{RPAr1}}, \tag{1.4-25}$$

in analogy to the adiabatic connection for the total correlation energy. To obtain the HOT correction we approximate two quantities, $\hat{b} \approx 0.5$ and $\Delta U_c[f_{xc}]^{bRPAr1} \approx \Delta U_c[f_{xc}]^{RPAr2}$. Then we get the following expression for correlation beyond RPAr as, $\Delta E_c[f_{xc}]^{bRPAr1} \approx \Delta E_c[f_{xc}]^{HOT} = 0.5\Delta U_c[f_{xc}]^{RPAr2}$. While $\hat{b}$ can in principle be computed correctly for any system, we find that approximating it to 0.5 is surprisingly robust and yields acceptable accuracy. In fact for several systems we find that the exact $\hat{b}$ defined in this way for approximate kernels is around 0.5. Furthermore, by comparing

to the properly integrated RPAr-n corrections of Eq. 1.4-22, this approximation for $\hat{b}$ seems to compensate for neglecting the third and higher order terms in the expansion of the RPAr correlation energy. The total correlation energy within the HOT approximation is computed as, $E_c[f_{xc}]^{HOT} = {E_c}^{RPA} + \Delta E_c[f_{xc}]^{RPAr1} + 0.5\Delta U_c[f_{xc}]^{RPAr2}$ where $\Delta U_c[f_{xc}]^{RPAr2} = \int_0^\infty < V\hat{\chi}f_{xc}\hat{\chi}f_{xc}\hat{\chi} > \frac{d\omega}{2\pi}$. For spin-unpolarized systems, or spin-independent kernels, the coupling strength integral for $\Delta E_c[f_{xc}]^{RPAr1}$ can be taken analytically for exchange-like kernels, meaning only one diagonalization of $\hat{\chi}^\lambda$ at $\lambda = 1$ is needed to compute the correlation energy, thus avoiding instabilities that come from having to diagonalize a response function that directly includes f_{xc}.

The reduction in computational cost for periodic boundary conditions is related to the reduced amount of time needed for diagonalization of $\hat{\chi}^\lambda$ in the reciprocal lattice basis, which is not rate-determining as the cost to build $\hat{\chi}^{KS}$ is quartic in a plane-wave basis. However, for systems such as metals where dense k-mesh samplings are needed for converged results, the reduction can be appreciable since the savings are per q-point. Exchange-correlation kernels or spin-polarized systems with any kernel still require numerical integration over λ within RPAr, as implemented using the density-density response function, so there is no reduction in computational cost, however instabilities are still avoided since only $\hat{\chi}^\lambda$ needs to be diagonalized. The RPA and beyond RPA corrections are obtained simultaneously and one does not need to perform two separate calculations in order to determine the behavior of each method. Instead, the total energy is a sum of separate pieces and the impact of the kernel compared to RPA can be directly determined.

1.4.3 Brief discussion of different kernels

The adiabatic equation to the kernel is $f_{xc}(\mathbf{r}, \mathbf{r}') = \frac{\delta v_{xc}(\mathbf{r}')}{\delta n(\mathbf{r})}$ where v_{xc} is the exchange-correlation potential of DFT. Hence LDA, PBE approximations in DFT leads to ALDA, APBE kernels. Kernels can be spatially renormalized and result in to rALDA[*Olsen*

and Thygesen, 2012,0], rAPBE[*Olsen and Thygesen*, 2014b] kernels. This renormalization eliminates the divergence of the pair-correlation function at the origin i.e., at $\mathbf{r} = \mathbf{r}'$. The RPA correlation for different densities of the homogeneous gas can not recover the exact uniform electron gas correlation energies for those densities. A non-local, dynamical and/or energy-optimized approximation for f_{xc} has been found to correct deficiencies of the RPA when calculating the correlation energy of the homogeneous electron gas (HEG) which is still the best benchmark for any new kernel development. Kernels can be static(frequency independent such as rALDA), dynamical(frequency dependent such as CPd)[*Constantin and Pitarke*, 2007], exchange-like (such as rAPBE), exchange-correlation like (such as CP07[*Constantin and Pitarke*, 2007]) and so on. In general adding kernels to RPA corrects the shortcoming of RPA for describing short range interactions.

CHAPTER 2

STRUCTURAL PHASE TRANSITIONS W.R.T SEMILOCAL FUNCTIONALS AND LONG-RANGE DISPERSION CORRECTIONS

2.1 Introduction

In this chapter, we have assessed the performance of the most advanced meta-GGA semilocal functional with dispersion corrections and have compared it to the experiment for structural phase transition pressures.[*Sengupta et al.*] The structural phase transition of solids is a fascinating phenomenon which has large theoretical and practical importance. Space-group symmetry and associated internal structural parameters change from one crystal structure to another with the external influence of, for example, temperature or pressure. Temperature or pressure induced structural phase transitions can change the electronic structures of the corresponding materials, such as from insulator to metal and vice versa, or it may change the band structures of the insulating or metallic state resulting in a change in band-gap or conductance. Structural phase transitions also sometimes lead to different magnetic states (e.g. antiferromagnetic to paramagnetic)[*Radaelli et al.*, 1997]. Hence control of structural phase transitions presents many potential applications in electronics, optics and other relevant fields.[*Kang et al.*, 2014; *Kato et al.*, 2003; *Vlasko-Vlasov et al.*, 2000] Since it is challenging to experimentally determine coexistence temperatures or pressures of two different structural phases of a solid, a robust theoretical method is needed.

In order to predict accurate transition pressures for structural phase transitions

in solids, accurate equilibrium geometries of and energy differences between the respective phases are required. Density functional approximations such as from the local density approximation (LDA) and generalized gradient approximations (GGA) yield reasonably accurate structures[*Perdew et al.*, 1992], but tend to underestimate the energy difference between low and high pressure phases.[*Mujica et al.*, 2003; *Xiao et al.*, 2012a] One of the most fundamental aspects of density functional theory is the self-interaction error[*Zhang and Yang*, 1998] (SIE), also known as the delocalization error. Hartree-Fock (HF) is a one-electron, self-interaction error free method by construction, and like the HF method, exact density functional theory would also be SIE free. However, for practical approximate density functionals some part of the SIE remains.[*Perdew and Zunger*, 1981a] This leads to a considerable reduction of the accuracy for the description of a variety of physical processes.[*Mori-Sánchez et al.*, 2006] Systems with d or f electrons containing both localized orbitals and delocalized orbitals are genuinely plagued by the SIE.[*Schmidt and Kümmel*, 2016] A natural solution to these challenges, the adiabatic connection fluctuation-dissipation (ACFD) formulation of density functional theory (DFT), is constructed from a self-interaction free exchange energy and a non-local correlation energy that directly accounts for dispersion.[*Eshuis et al.*, 2012a; *Ren et al.*, 2012a] But first we wanted to test the highest order semilocal functional meta-GGA SCAN's performance for determining the phase transition pressure and then analyze it by adding a long range dispersion correction to it which provides a systematic improvements of the phase transition pressure for wide varities of materials with considerable accuracy. Dispersion correction can be added to semilocal density functionals.

2.2 Choice of materials and their brief history

We have compiled a small but representative set of bulk solids to assess the performance of the methods.

2.2.1 Silicon and Germanium

The diamond structures of silicon (Si) and germanium (Ge) are indirect band-gap semiconductors, and at high pressures their properties are remarkably similar though not identical. The semiconducting diamond phases of both materials undergo a transition to the metallic beta-tin (β-Sn) phase under pressures in the range of 10 – 14 GPa.[*Mujica et al.*, 2003] The beta-tin phase was predicted to be the the most favored structure of Si and Ge at high pressure among several other possibilities by first principles calculations in agreement with experiment.[*Yin and Cohen*, 1982] The relative stability of the cubic diamond and beta-tin phases of Si and Ge has been the subject of previous theoretical studies and has become a benchmark for several theoretical methods.[*Dal Corso et al.*, 1996; *Moll et al.*, 1995] Still, more accurate theoretical methods are welcome to resolve the descrepancies between Monte Carlo and density functional calculations.[*Xiao et al.*, 2012a]

2.2.2 SiC

Silicon Carbide (SiC) is an indirect band gap semiconductor and crystallizes in the zinc blende (ZnS) structure under normal conditions. Due to its stability over a wide range of temperatures and pressures, it has been used in high power electronics and in integrated circuits as a reliable base to support other materials.[*Kashyap et al.*, 2013] It is also frequently used in composite materials and related applications as a hard ceramic material.[*Schwetz*, 2000] Theoretical studies first showed that among several possible high-pressure structures, rocksalt is the most energetically stable for SiC.[*Chang and Cohen*, 1987; *Karch et al.*, 1994] The rocksalt phase is also metallic, in contrast to the low-pressure phase. Yoshida *et al.* later reported an experimental structural phase transition from zinc blende to metallic rocksalt at 100 GPa.[*Yoshida et al.*, 1993] Further theoretical studies have confirmed these earlier works, but theoretical values largely underestimate the experimental transition pressure[*Catti*, 2001a;

Miao and Lambrecht, 2003] most likely due to a thermodynamic barrier that must be overcome in the experiment[*Durandurdu*, 2007], but not in the calculations.[*Miao and Lambrecht*, 2003]

2.2.3 Gallium Arsenide

Gallium Arsenide (GaAs) is a wide band gap semiconductor and crystallizes in the zinc blende (ZnS) structure under normal conditions. Due to its higher electron mobility and higher saturated electron velocity it is suitable to operate at high frequencies.[*Baliga*, 1989; *Blakemore*, 1982] Due to its direct bandgap, GaAs shows strong photoemission as well.[*Bachelet and Christensen*, 1985; *Eastman et al.*, 1974] These properties, coupled with a high dielectric constant, are the reasons why GaAs is widely used in integrated circuits, interstellar electronics, optics, and solar cells.[*Blakemore*, 1982; *Crowe et al.*, 1992; *Curtice*, 1980; *Gobat et al.*, 1962; *Van Tuyl et al.*, 1982] Minomura and Drickamer observed a pressure induced phase transition in GaAs[*Minomura and Drickamer*, 1962] at 24 GPa by high-pressure electrical resistance experiments. Afterwords, many theoretical and experimental studies confirmed that GaAs undergoes a structural phase transition from the semiconducting zinc blende structure to a metallic state with orthorhombic symmetry at 17 GPa under compression.[*Mujica et al.*, 2003; *Weir et al.*, 1989] Finally McMahon *et al.* correctly identified the structure of that metallic phase as the site ordered Cmcm structure.[*Nelmes and McMahon*, 1995] Besson *et al.* also extensively studied forward and reverse transitions experimentally between low and high-pressure phases using optical-transmittance measurements, Raman scattering, and X-ray absorption techniques, suggesting that the thermodynamic transition pressure of ZnS to Cmcm phase of GaAs at about 13.5 GPa around 300 K.[*Besson et al.*, 1991]

2.2.4 Silicon Dioxide

Silica or Silicon Dioxide (SiO_2) is used in a variety of applications such as in the production of glass or in optical fibers for telecommunications.[*Atkins et al.*, 2010] The pressure induced phase transition from the low-pressure quartz phase to the high-pressure stishovite phase at around 7 GPa is accompanied by a change in coordination of the Si atoms[*Xiao et al.*, 2012a], and a large increase in the hardness of the material. Xiao *et al.*[*Xiao et al.*, 2012a] demonstrated that most semilocal functionals struggle to predict accurate structural parameters or phase transition parameters, with the execption of the PBE GGA [*Perdew et al.*, 1996a] and a certain class of meta-GGAs.[*Xiao et al.*, 2013] Though RPA predicts accurate structural properties for the two materials, it underestimates the energy difference between the phases, resulting in an underestimation of the transition pressure[*Xiao et al.*, 2012a]. The authors of Ref. [*Xiao et al.*, 2012a] suggest that this apparent failure of RPA is likely due to an imperfect cancellation of errors, and we further support this assessment below by demonstrating the impact of an exchange-correlation kernel on the computed transition pressure and energy difference between phases.

2.2.5 Lead (Plumbum)

Lead (Pb) is a metal and crystallizes in the FCC structure under normal conditions, but a transition to the HCP structure is observed at 14 GPa.[*Mao et al.*, 1990; *Vanderborgh et al.*, 1990] The volume reduction is very small at the transition and therefore there is a large region of phase coexistence, consistent with a very small enthalpy difference between the phases over a large pressure interval. Liu *et al.* [*Liu et al.*, 1991] studied the stability of Pb at high pressures using plane wave pseudopotential methods, including scalar-relativistic and spin-orbit effects. The three structural phases FCC, HCP, and BCC were found to be very close in energy, but nonetheless the sequence of transitions was correctly described, as well as the struc-

tural properties of the phases. Hermann *et al.* also studied Pb with and without relativistic effects and found that the structural properties of the HCP phase are much more strongly affected than the FCC phase.[*Hermann et al.*, 2010]

2.2.6 Boron Nitride

Diamond and cubic boron nitride (BN) are similar materials; both of them are extremely hard and have very high melting point.[*Vel et al.*, 1991] They are mostly chemically inert and have a large thermal conductivity.[*Vel et al.*, 1991] Cubic BN (c-BN) does not dissolve in iron and steel and thus is an excellent material for the protective coating of heavy tools.[*Vel et al.*, 1991] It has a wide band gap and relatively small dielectric constant, so it has great applications in the domain of UV optics and high temperature microelectronics.[*Davis*, 1991; *Vel et al.*, 1991] DFT and experimental studies indicate that the diamond-like c-BN is more stable than the graphite-like hexagonal (h-BN).[*Furthmüller et al.*, 1994; *Solozhenko et al.*, 1999; *Wentzcovitch et al.*, 1988] Due to the heteropolarity effect, the equilibrium energy difference of the cubic and hexagonal phases of BN is much larger than those found between the diamond and graphite phases in carbon.[*Mujica et al.*, 2003] Even including the effects of zero-point energy and the finite temperature using the quasiharmonic approach, Albe *et al.*[*Albe*, 1997] and Kern *et al.*[*Kern et al.*, 1999] did not find very accurate transition pressure compared to the experiment.

2.2.6.1 Carbon

The diamond and graphite phases of carbon (C) are very different from each other, unlike BN. Diamond is an indirect, wide band gap insulator while graphite is a layered, zero band gap semimetal. Diamond has a large thermal conductivity and is mostly chemically inert like cubic BN. Diamond is also a very hard material due to its strong sp^3 hybridization.[*Mujica et al.*, 2003] Graphite, however, is a soft

and stiff material with very high thermal stability, high thermal conductivity and electrical conductivity due to the inability of phonons to propagate quickly between layers with weak interaction, and availability of delocalized free electrons between the layers respectively.[*Mujica et al.*, 2003] Experiments have confirmed that the graphite is the stable phase under normal condition, and that it can undergo a phase transition to the diamond phase around 1.7 GPa at 0 K and around 12 GPa at 5000 K.[*Bundy et al.*, 1996] Also the energy difference between the lower pressure graphite and higher pressure diamond is very small, around $5 - 20$ meV at 0 K.[*Harl and Kresse*, 2009] Most of the semilocal functionals either yield the wrong ordering of the phases with respect to experiment or overestimate the energy difference.[*Furthmüller et al.*, 1994; *Mailhiot and McMahan*, 1991] Even RPA can not provide the correct ordeing of the phases and energy difference, and it shows that those phases are nearly degenerate at 0 K.[*Harl and Kresse*, 2009]

Recently, Cui *et al.* showed that the relative stability of TiO_2 in the rutile and anatase structure is correctly described by RPA. They further concluded that including the zero-point energy and finite-temperature effects based on the harmonic approximation, increases the relative stability of the rutile phase compared to anatase phase, and leads to a better quantitative agreement with experimental measurements.[*Cui et al.*, 2016] Whittleton et. al. also found that thermal corrections are very important for an accurate energy ranking of the polymorphs of organic molecular crystals.[*Whittleton et al.*, 2017] In their work, 4-hydroxythiophene-2-carbonitrile's experimental structure is only correctly identified once a quasi-harmonic estimate of the vibrational free-energy contribution is included. Our results also show that when the energy difference between the phases for bulk solids is close to zero, the temperature corrections are crucial for determining the most stable phase.

In the following sections, we briefly describe the computational details in Section 2.3, and present the results for each system in Section 2.4. A brief discussion

and conclusions are then given in Section 2.5.

2.3 Computational Details

The calculations were performed using a modified version of GPAW,[*Enkovaara et al.*, 2010; *Mortensen et al.*, 2005] a python-based software built on the Atomic Simulation Environment (ASE) package[*Bahn and Jacobsen*, 2002] and utilizing the projector augmented wave (PAW) method.[*Blöchl*, 1994] GPAW was used to compute the LDA[*Ceperley and Alder*, 1980; *von Barth and Hedin*, 1972] and PBE[*Perdew et al.*, 1996a] results discussed below. The Gamma-centered Monkhorst-Pack[*Monkhorst and Pack*, 1976] k-meshes were used throughout. Results from the strongly constrained and appropriately normed (SCAN) meta-GGA were obtained with the VASP [*Kresse and Hafner*, 1993] software package using normal PBE POTCARs which include kinetic energy density component for B, N, Si, O, C, and normal PBE POTCARs which include fully occupied d orbital electrons as well as kinetic energy density component for Ga, As, Pb, Ge. We have carefully done convergence tests for each material with LDA, PBE, and SCAN with regard to the cutoff energy of the input wavefunctions and the k-mesh. All parameters were chosen to yield errors on the order of 0.02 eV per functional unit or less. The converged parameters we used are reported in the Table 2.1. Note that, LDA, PBE were applied within GPAW, whereas SCAN was applied within VASP.

In order to apply density functional theory to real systems, an approximation for the unknown exchange-correlation (xc) energy is needed. Within the hierarchy of approximate functionals[*Perdew et al.*, 2001], the local density approximation[*von Barth and Hedin*, 1972] (LDA) depends only on the electron density. Higher-level functionals, such as GGAs or meta-GGAs, incorporate gradients of the density and dependence on the kinetic-energy density, respectively. Through its dependence on the kinetic energy density, the SCAN meta-GGA is able to capture intermediate-range van

Table 2.1: Convergence parameters used in our calculations of the transition pressures for semilocal functionals.

Materials	**LDA**		**PBE**		**SCAN**	
	ecut(eV)	**k-mesh**	**ecut(eV)**	**k-mesh**	**ecut(eV)**	**k-mesh**
Si (Diamond)	800	10x10x10	800	10x10x10	800	12x12x12
Si (Beta-tin)	800	10x10x12	800	10x10x12	800	10x10x12
Ge (Diamond)	650	12x12x12	650	12x12x12	600	12x12x12
Ge (Beta-tin)	700	10x10x12	700	10x10x12	600	10x10x12
SiC (ZnS)	800	12x12x12	800	12x12x12	800	12x12x12
SiC (Rocksalt)	800	12x12x12	800	12x12x12	800	12x12x12
GaAs (ZnS)	600	6x6x6	600	6x6x6	600	12x12x12
GaAs (Cmcm)	600	8x7x9	600	8x7x9	600	8x7x9
SiO_2 (Quartz)	1000	4x4x2	1000	4x4x2	800	4x4x2
SiO_2 (Stishovite)	1000	5x5x6	1000	5x5x6	800	5x5x6
Pb (Fcc)	1000	20x20x20	1000	20x20x20	1000	12x12x12
Pb (Hcp)	1000	18x18x8	1000	18x18x8	1000	14x14x6
C (Graphite)	1200	18x18x8	1200	18x18x8	600	14x14x6
C (Diamond)	1200	12x12x12	1200	12x12x12	600	12x12x12
BN (Cubic)	1200	6x6x6	1200	6x6x6	600	12x12x12
BN (Hexagonal)	950	8x8x3	950	8x8x3	600	14x14x6

der Waals interactions, but is lacking long-range weak interactions[*Brandenburg et al.*, 2016b; *Peng et al.*, 2016]. In order to incorporate long-range dispersion, methods such as Vydrov and van Voorhis's VV10 and revised VV10 (rVV10) were developed to provide the missing dispersion. Dispersion is included by adding a non-local correlation component to the semilocal exchange-correlation energy such that $E_{xc} = {E_{xc}}^{0} + {E_c}^{nl}$, where E_{xc} is the total exchange correlation energy.[*Sabatini et al.*, 2013; *Vydrov and Van Voorhis*, 2010] Both the original VV10 and rVV10 have the flexibility to be tuned to different semilocal functionals[*Björkman et al.*, 2012], though we will only explore their combination with SCAN and PBE, and take the relative results compared to the bare functional as indicative of the performance of any semilocal functional. We note, however, that the addition of rVV10 to SCAN does not contaminate the accurate intermediate-range vdW description of the bare SCAN functional.[*Peng et al.*, 2016] Grimme's empirical dispersion correction scheme was also explored in both the D2[*Grimme*, 2006] and D3[*Grimme et al.*, 2010,0] variants.

From the phonon spectrum, the zero-point energy contribution and finite-temperature corrections can be obtained to study temperature-dependent transition pressures. We

have calculated the phonon spectra from first-principles calculations based on DFT as implemented in VASP[*Kresse and Hafner*, 1993]. Density functional perturbation theory[*Baroni et al.*, 2001; *Gonze and Lee*, 1997] has been used to compute the dynamical matrices for all the materials. Then we used our own code to calculate the temperature dependent phonon entropy contribution from the above data as well as temperature dependent electron entropy from the electronic density of states (DOS) data also generated using VASP. We used the same cutoffs, k-meshes, and PAWs[*Kresse and Joubert*, 1999] for the phonon calculations as for our zero-temperature energy calculations. Previous studies have shown that different density functionals produce similar results for the zero-point energy[*Landerville et al.*, 2010] (ZPE) and thermal corrections to the transition pressure[*Xiao et al.*, 2012a], hence we have used only PBE to compute the phonons. To compare with the existing literature equillibrium cell volumes, the results in Table 2.2 do not include the shifts due to the phonon corrections.[*Xiao et al.*, 2012b]

The Gibbs free energy is, $G(V,T) = E(V,T) - TS(V,T) + P(V,T)V = F(V,T) + P(V,T)V$, where $E(V,T)$ is the internal energy and $F(V,T) = E(V,T) - TS(V,T)$ is the Helmholtz energy. At the transition pressure, the difference in the Gibbs free energies for the two phases should be equal to zero. At zero temperature, the Gibbs free energy reduces to the enthalpy, $H(V) = E(V) + P(V)V$, and so the transition pressure is the pressure where the enthalpy difference between phases is equal to zero. $E(V)$ and $P(V)$ can also be denoted as $E(V, T = 0)$ and $P(V, T = 0)$, emphasizing that they are zero-temperature energy and pressure.

At zero temperature, structural parameters for each phase, such as the equilibrium cell volume (V_0), and corresponding equilibrium energy (E_0), bulk modulus (B_0), and pressure derivative of the bulk modulus (B_0'), can be evaluated by fitting the energy-volume (E-V) data generated through density functional theory to the standard third-order Birch-Murnaghan (BM) equation of state (EOS) given by,

$$E(V) = E_0 + \frac{9B_0V_0}{16}([(\frac{V_0}{V})^{2/3} - 1]^3 B_0' + [(\frac{V_0}{V})^{2/3} - 1]^2[6 - 4(\frac{V_0}{V})^{2/3}]) \,. \tag{2.3-1}$$

The pressure can also then be analytically computed, after determining the four fitting parameters (E_0, B_0, V_0, B_0') from Eq. (2.3-1), as

$$P(V) = \frac{3B_0}{2}[\frac{V_0}{V}^{7/3} - \frac{V_0}{V}^{5/3}](1 + \frac{3}{4}(B_0' - 4)[\frac{V_0}{V}^{2/3} - 1]) \ . \tag{2.3-2}$$

The transition pressures and volumes are determined by a brute force numerical minimization of the enthalpy or Gibbs free energy difference between phases at zero and finite temperature, respectively. We compute the enthalpies of the respective phases at their corresponding equilibrium volumes with the help of Eq. (2.3-1) and Eq. (2.3-2). Starting from a guess for the transition pressure, $P_{t,0} = 0.5\frac{\delta E_0}{\delta V_0}$, the pressure is iteratively increased or decreased to force the enthalpy difference between the phases to zero. We use a convergence threshold of at least 10^{-4} eV per atom to ensure tight convergence of the phase transition parameters.

To include the zero point motion and thermodynamic contributions from vibrational degrees of freedom, we use the Helmholtz free energy. For a lattice, the Helmholtz free energy is given within the quasi-harmonic approximation[*Althoff et al.*, 1993; *Hamdi and Meskini*, 2010; *Mounet and Marzari*, 2005; *Pavone et al.*, 1998]

(QHA) as

$$\begin{aligned} F(V,T) &= E(V,T) - TS(V,T) \\ &= E(V) + \sum_{q,j} \frac{\hbar\omega_{q,j}(V)}{2} \\ &+ k_B T \sum_{q,j} ln[1 - exp(-\frac{\hbar\omega_{q,j}(V)}{k_B T})] \\ &= E(V) + k_B T \sum_{q,j} ln[2sinh(\frac{\hbar\omega_{q,j}(V)}{2k_B T})] \ , \end{aligned} \tag{2.3-3}$$

where E(V,T) is the lattice crystal energy at a specified volume and temperature, and $\omega_{q,j}(V)$ is a computed phonon frequency.

At a finite temperature, the Gibbs free energy is $G(V,T) = F(V,T) + VP(V,T)$. $P(V,T)$ should be obtained from $F(V,T)$ as,

$$P(V,T) = -(\frac{\partial F}{\partial V})_T \, . \tag{2.3-4}$$

For that purpose, we have done the EOS fitting of $F(V,T)$ from Eq. (2.3-3) to an isothermal third-order BM EOS,

$$F(V,T) = F_{0T} + \frac{9B_{0T}V_{0T}}{16}[(\frac{V_{0T}}{V})^{2/3} - 1]^3 B'_{0T} \tag{2.3-5}$$

$$+ [(\frac{V_{0T}}{V})^{2/3} - 1]^2 [6 - 4(\frac{V_{0T}}{V})^{2/3}] \, , \tag{2.3-6}$$

where F_{0T} is the Helmholtz free energy at the equilibrium volume, and each of the fitting parameters (F_{0T}, B_{0T}, V_{0T}, B'_{0T}) depend implicitly on the temperature (indicated by the subscript) due to the phonon correction. Analogously, the pressure is

then obtained from Eq. (2.3-7) using the isothermal EOS fitting parameters

$$\begin{aligned} P(V,T) &= -(\frac{\partial F}{\partial V})_T \\ &= \frac{3B_{0T}}{2}[(\frac{V_{0T}}{V})^{7/3} - (\frac{V_{0T}}{V})^{5/3}] \\ &(1 + \frac{3}{4}(B'_{0T} - 4)[(\frac{V_{0T}}{V})^{2/3} - 1) \ . \end{aligned} \tag{2.3-7}$$

After that, the same numerical procedure is used to obtain the phase transition pressure as for the zero-temperature case.[*Gaál-Nagy et al.*, 1999]

In principle, the approximation used to compute E_{xc} for the electronic energy should also be used to compute the phonon spectra, however this is not possible for many meta-GGA functionals because analytic second derivatives of the potential energy with respect to nuclear positions have not been implemented in any code. Performing finite differences would be too expensive for the latter methods. Since the phonon spectrum within SCAN is unavailable, we have elected to use the phonon spectra predicted by PBE to compute all of the thermal effects in our work. It was confirmed that this was a reasonable approach for BN, GaAs, and Si by computing the LDA phonon spectra and adding LDA thermal effects. The resulting transition pressures were negligibly different from the reported results herein using the PBE phonon spectra.

2.4 Results

It is well known that LDA and PBE tend to underestimate and overestimate structural parameters of molecules and materials[*Haas et al.*, 2009; *Perdew et al.*, 1992; *Rappoport et al.*, 2006], while SCAN was recently demonstrated to improve upon both of these methods for energetics and structures.[*Sun et al.*, 2016] Our results for the materials studied herein reflect these same trends, with SCAN being the most accurate semilocal functional for predicting the equilibrium structural parameters, as

Table 2.2: Equilibrium cell volumes (Å^3) obtained from the EOS fits for each method. SCAN tends to be the most accurate semilocal functional, while PBE overestimate and LDA underestimates.

Materials	**LDA**	**PBE**	**SCAN**	**Expt**[1]
Si (Diamond)	39.503	41.048	39.976	40.037
Si (Beta-tin)	59.540	61.583	59.772	55.820[*McMahon et al.*, 1994]
Ge (Diamond)	44.644	47.942	45.287	45.271
Ge (Beta-tin)	71.655	77.030	74.214	74.169
SiC (ZnS)	20.408	21.148	20.607	20.693
SiC (Rocksalt)	16.260	16.868	16.342	16.554[*Catti*, 2001b]
GaAs (ZnS)	44.684	48.028	45.592	45.138
GaAs (Cmcm)	143.509	154.249	147.248	
SiO_2 (Quartz)	36.822	40.351	37.357	37.803
SiO_2 (Stishovite)	23.351	24.445	23.284	23.325
Pb (Fcc)	28.908	31.815	30.648	30.010
Pb (Hcp)	57.468	63.326	60.976	48.530
C (Diamond)	11.024	11.403	11.240	11.345
C (Graphite)	34.548	35.599	34.935	36.615
BN (Cubic)	11.482	11.915	11.742	11.664
BN (Hexagonal)	35.500	36.683	35.963	36.701

shown in Table 2.2. Comparing all methods, SCAN is the most accurate for predicting structural properties, while PBE is the worst. Consequently, the performance for the transition pressure shows similar trends among semilocal methods, though there are some differences for comparing performance across all methods. We note that our SCAN results for several materials are in good agreement with those of Ref. [*Shahi et al.*, 2018], though a $\sim$ 4 GPa discrepancy for Pb was discovered due to slightly different procedures used to obtain the EOS fit for the HCP phase.

To compare the various electronic structure methods we can divide the materials into three broad groups based on their phase transitions. First is the phase transition between two highly symmetric phases such as in Si, Ge, and SiC. The second group concerns phase transitions between two dissimilar phases comprised of at least one low-symmetry phase such as in GaAs (low-symmetry phase: cmcm) and SiO_2 (low-symmetry phases: quartz, stishovite). Lastly, there are the special cases, such as the metal to metal phase transition of Pb, and the phase transition between two nearly degenerate phases such as in C and BN.

Table 2.3: Transition pressure (GPa) without temperature correction for semilocal functionals.

Materials	**LDA**	**PBE**	**SCAN**	**Expt**[*Mujica et al.*, 2003][1]
Si	7.3	9.7	14.5	12.0
Ge	6.5	8.1	11.3	10.6
SiC	61.0	65.8	74.1	100.0
GaAs	10.5	12.8	17.1	15.0
SiO_2	–0.7	5.8	4.6	7.5[*Hamann*, 1996]
Pb	11.1	13.6	16.4	14.0
C	–0.6	6.1	4.6	3.7
BN	–3.3	3.2	2.8	5.0

2.4.1 Phase transitions between highly symmetric phases

Considering the first group of materials and semilocal functionals at zero temperature, Table 2.3 illustrates that SCAN overestimates the transition pressures of Si and Ge in comparison to experiment, while PBE and LDA underestimate them (experimental values are given in Table 2.7). Our results are in good agreement with previous studies using the latter two functionals.[*Mujica et al.*, 2003; *Xiao et al.*, 2013] Our SCAN results yield an energy difference between phases of 0.417 eV per functional unit for Si which is equivalent to what Sun *et al.* reported in their previous study of this system[*Sun et al.*, 2016], see Table 2.4.

Table 2.4: Equilibrium energy differences without temperature corrections for semilocal functionals, reported in eV/functional unit. Here functional unit also implies formula unit.

Materials	**LDA**	**PBE**	**SCAN**
Si	0.212	0.289	0.417
SiC	1.348	1.471	1.631
Ge	0.168	0.220	0.265
GaAs	0.525	0.668	0.825
SiO_2	–0.061	0.489	0.356
Pb	0.010	0.012	0.015
C	–0.013	0.120	0.088
BN	–0.130	0.126	0.105

Comparing all semilocal methods, LDA and PBE are clearly inferior to the higher

order method SCAN. As discussed above, there is a remarkably large error for all methods in comparison to experiment for the transition pressure of SiC. Thus we find it more appropriate to compare electronic structure methods amongst themselves instead of to experiment, since the computed values all correspond to the same thermodynamic process and do not consider the impact of transition barriers on the transformation. In this way, the analysis for Si and Ge is completely transferrable to SiC and hence why we have grouped them together; SCAN yields a small overestimate of the transition pressure and, LDA and PBE are clear underestimators for the same.

We have also tested the effect of adding different long-range dispersion corrections for Silicon as a representative example of the group of materials which undergoes phase transition from one highly symmetric phase to another highly symmetric phase discussed in the previous chapter. Numerical results are presented in Table 2.5 and Table 2.6 below.

Table 2.5: Transition Pressure (GPa) with dispersion correction at zero temperature.

Materials	**PBE**	**+D2**	**+D3**
Si	9.73	9.03	6.47
GaAs	12.75	10.71	9.97
SiO_2	5.80	2.88	2.85
Pb	13.86	10.26	6.02
BN	3.17	–2.08	0.17

Table 2.6: Transition Pressure (GPa) with dispersion correction at zero temperature.

Materials	**SCAN**	**+D3**[*Brandenburg et al.*, 2016b]	**+rvv10**[*Peng et al.*, 2016]
Si	14.51	13.65	12.82
GaAs	17.07	16.43	15.75
SiO_2	4.57	3.76	3.34
Pb	16.35	15.84	14.95
BN	2.74	1.97	1.41

We have found that the most recent version of Grimme's empirical dispersion correction scheme, DFTD3[*Grimme et al.*, 2010,0], when parametrized for SCAN[*Brandenburg*

et al., 2016b] yields similar shifts in the equilibrium volumes, energy difference between phases and subsequently the transition pressures compared to previous calculations using PBE and DFTD2[*Grimme*, 2006]. The same is true for more advanced dispersion corrections when added to SCAN, such as for rVV10[*Peng et al.*, 2016; *Sabatini et al.*, 2013], reinforcing the conclusion of Ref. [*Xiao et al.*, 2013] that adding empirical dispersion for covalent materials is not always pertinent, especially in highly symmetric solids.

With the addition of finite temperature corrections from the computed phonon spectra of PBE, the transition pressures for Si, Ge, and SiC are all shifted to smaller values indicating the stability of the high-temperature phase in each case, Table 2.7. The shifts are fairly small here, and do not significantly change the relative trend amongst the functionals. SCAN is now closest to the experiment for Si and Ge, and, even for SiC, SCAN still remains close to the experimental method.

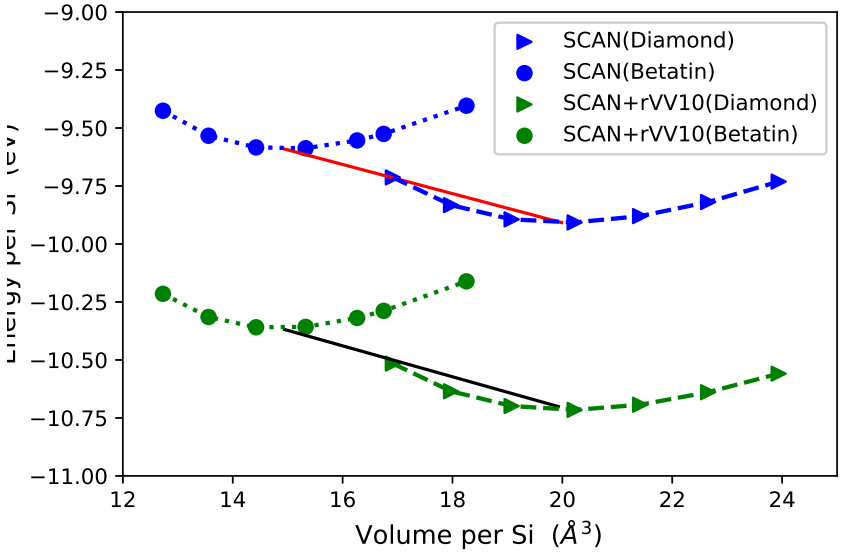

Figure 2.1: EV curve for diamond and betatin phases of Si with SCAN and SCAN+rvv10.

Table 2.7: Transition pressures (GPa) including temperature corrections at room temperature, 300 K for semilocal functionals.

Materials	**LDA**	**PBE**	**SCAN**	**Expt**[*Mujica et al.*, 2003]
Si	6.3	8.5	13.8	12.0
Ge	5.6	7.1	10.4	10.6
SiC	56.4	61.4	69.1	100.0
GaAs	9.4	11.6	16.1	15.0
SiO_2[1]	-0.1	6.4	5.2	7.5[*Hamann*, 1996]
Pb	17.8	21.7	22.2	14.0
C	3.1	9.8	8.3	3.7
BN	0.1	6.5	6.1	5.0

2.4.2 Transitions involving a low-symmetry phase

For the second group of materials an accurate treatment of correlation at all ranges can be necessary to produce accurate results, though the details of the electronic structure are also important. Similarly to the first group of materials without temperature corrections, SCAN is accurate but overestimates the experimental transition pressure of GaAs while PBE and LDA noticably underestimate it.

For SiO_2, the situation is noticably different than for the first group of materials or even GaAs. LDA completely fails for this system, yielding an incorrect phase ordering compared to experiment even though the equilibrium volumes are acceptably accurate. PBE serendipitously predicts a reasonably large transition pressure for this system within 2 GPa of experiment, though it systematically overestimates the structural parameters. Our results for these functionals closely match those from previous studies.[*Mujica et al.*, 2003; *Xiao et al.*, 2013] In this material SCAN does not systematically improve upon PBE for the equilibrium energy difference or transition pressure, though the equilibrium volumes are much more accurate compared to experiment. One possible source of difficulty with the non-empirical semilocal functionals are the strongly polar (almost ionic) bonds in silica due to the large difference in electronegativity between Si and O, causing self-interaction error.

An essentially rigid shift is also introduced to the results of the semilocal function-

als of the previous chapter with the addition of an empirical dispersion correction, see the Table 2.5 and Table 2.6 for numerical results for SiO_2. As reported in Ref. [*Xiao et al.*, 2013], addition of dispersion for SiO_2 reduces the equilibrium volumes and equilibrium energy differences, though we do find that the magnitude of the shift depends on the damping and functional for which the correction was parametrized. For instance, in Ref. [*Xiao et al.*, 2013] addition of D2 to TPSS produced a large negative shift in the transition pressure which actually results in a final transition pressure which is slightly negative. With the more recent D3 scheme for both PBE and SCAN, the shifts are still 1-3 GPa to smaller pressures, and the zero damping scheme tends to produce smaller shifts than the Becke-Johnson (BJ) type damping[*Grimme et al.*, 2011]. Adding rVV10 to SCAN also results in shifts similar to D3 with BJ damping.

The addition of thermal corrections for GaAs and SiO_2 is also similar to that for the first group in that the thermal corrections typically introduce only a rigid shift in the performance of all the methods. For GaAs the finite-temperature corrections reduce the transition pressures while for SiO_2 they increase the pressure and energy difference mostly due to entropic effects.[*Lee and Gonze*, 1995; *Xiao et al.*, 2013] These shifts neither change the relative relationships between the functionals nor the experiment, and are not necessarily crucial for these materials where the energy gap between the phases is appreciable.

2.4.3 Special cases

The third group of materials are those for which there are some special circumstances which cause unexpected results or for which near degeneracies make it difficult to properly assess semilocal functionals. For Pb, a heavy Group IV element, relativistic effects can play an important role in determining the electronic structure. Though the PAW datasets that we have used include scalar relativistic effects for the core and valence electrons,[*Blöchl*, 1994; *Enkovaara et al.*, 2010] this may not be enough when

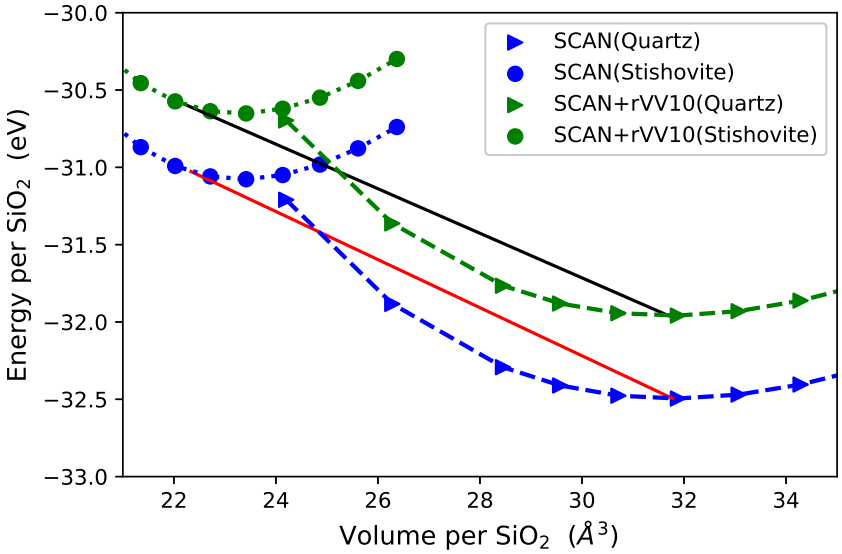

Figure 2.2: EV curve for quartz and stishovite phases of SiO_2 with SCAN and SCAN+rvv10

full relativistic effects in the valence are also crucial. For the FCC phase of Pb the relativistic treatment of the core electrons is sufficient, since for both semilocal and ACFD methods the performance trend for the structural parameters follows the other materials. For the HCP phase, however, full relativistic effect in the valence are sizeable,[*Hermann et al.*, 2010] and consequently all of the methods we applied yield large overestimates of the equilibrium volume.

The transition pressure predicted for Pb shows a remarkable cancellation of errors considering the gross overestimation of the HCP equilibrium volume. Without the temperature corrections, LDA, PBE, and SCAN all underestimate the experimental transition pressure, with PBE yielding a larger transition pressure than the other two.

Though non-relativistic methods are entirely appropriate for carbon and boron nitride materials, the near degeneracies at 0 K encountered for the cubic and hexagonal phases of these materials complicate the prediction of the pressure induced phase transitions. All of the methods produce reasonably accurate structures for both phases of C and BN, but the prediction for the relative stabilities and transition pressures has

proved to be challenging for some of the methods.

In particular, Table 2.4 shows that LDA fails to predict the proper phase ordering for both C and BN, as it did for SiO_2, and so the zero-temperature transition pressures are also inaccurate. PBE and SCAN both overestimate the transition pressure for C and underestimate it for BN, though SCAN is more accurate for C and PBE is more accurate for BN.

The addition of empirical dispersion was also explored for Pb and BN and is reported in the above tables. For Pb, adding the dispersion corrections also reduces the transition pressures. For PBE+D3 the reduction is close to 1.5 GPa, but for PBE+D2 it is closer to 4.5 GPa. Adding the D3 correction to SCAN hardly changes the SCAN result, however addition of rVV10 results in a 2 GPa reduction of the transition pressure bringing it close to that predicted by PBE+D2. Though addition of the dispersion corrections to Pb yields a reduction in the transition pressure similar to Zr, the addition of thermal corrections increases the transition pressure of Pb whereas it reduces the transition pressure of Zr.[*Xiao et al.*, 2013] Also the magnitude of the shift due to thermal corrections in Pb is much higher than that of Zr because of the presence of soft phonon modes.

The addition of thermal corrections for Pb, C, and BN tends to unilaterally destabilize the high-pressure phase resulting in a positive shift to the zero-temperature transition pressures. For Pb, which is typically considered a very soft metal, the thermal corrections from PBE unilaterally result in overestimates of the finite-temperature transition pressure for all methods, though the spread in the results is noticably decreased. Thus it is clear that the zero-temperature results benefit from cancellation of opposing effects generated by the stabilization due to relativity and destabilization due to phonons in the HCP phase.

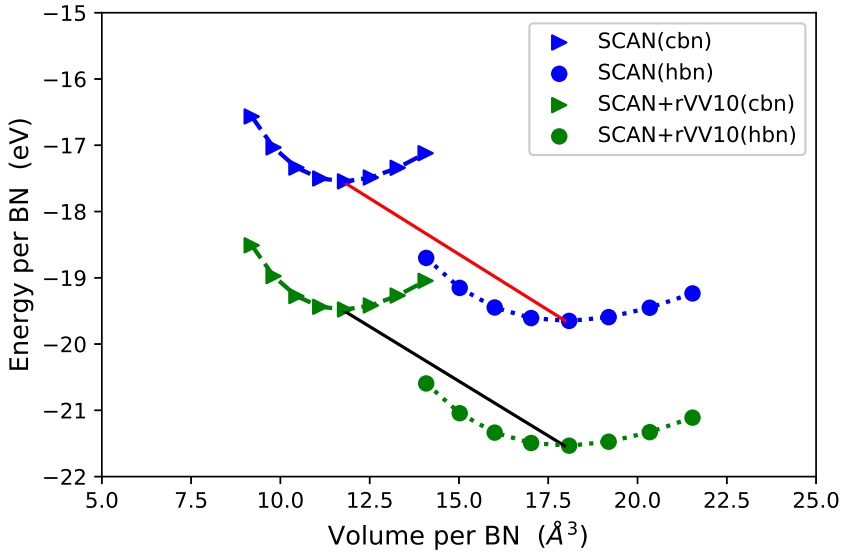

Figure 2.3: EV curve for cubic and hexagonal phases of BN with SCAN and SCAN + rvv10

2.5 Discussions and Conclusions

In this chapter, We evaluated the performance of LDA, PBE, SCAN, for the determination of structural properties and transition parameters of different phases. Both the zero-temperature electronic structure calculations of the ground state and the finite-temperature predictions with thermal corrections from phonons were compared with experimental results. For materials with two high-symmetry phases and an appreciable energy difference between phases, semilocal density functionals are usefully pretty accurate. For materials with dissimilar phases, semilocal functionals can struggle to produce systematic results from one functional to the next, especially in cases such as SiO_2 where self-interaction error can play an important role. For materials which require special consideration to understand their behavior, SCAN can also be a practical choice for compromising between speed and accuracy. Since SCAN also accounts for different ranges of electronic interactions, it delivers the highest quality semilocal results. Through its meta-GGA form SCAN captures the

usual short-ranged exchange and correlation effects of earlier semilocal functionals. Furthermore, it includes medium-range van der Waals interactions that are missing in, e.g., LDA or PBE. SCAN still benefits somewhat from residual self-interaction errors and a lack of long-range dispersion which tend to offset each other, since the former is repulsive and the latter attractive. Therefore we can recommend SCAN as a general method to represent semilocal functionals when exploring new materials or phase transitions. Thermal corrections and empirical dispersion were also explored as additional corrections to all methods and the semilocal functionals, respectively. We have found that addition of empirical long-range empirical dispersion corrections to the semilocal functionals generally tends to improve the results for simple materials but does not always provide reliable systematic corrections for asymmetric phases and special materials. The former can either stabilize or destabilize the high-pressure phase, but in general the shifts introduced by phononic corrections are smaller than the differences in performance for the various methods. For soft materials or those with near degeneracies, including the thermal corrections can be crucial to obtain results consistent with the experiment.

CHAPTER 3

PHASE TRANSITION PRESSURES WITH RPA AND BEYOND-RPA METHODS

3.1 Introduction

In this chapter, we have assessed the performance of the RPA and beyond RPA methods and have compared it to the experiment as well as semilocal cases, described in the previous Chapter 2 for structural phase transition pressures.[*Sengupta et al.*]

A natural solution to the shortcomings of semilocal density functionals in regard to inadequate description of van der Waals interactions for thses transition pressure challenges, is the adiabatic connection fluctuation-dissipation (ACFD) formulation of density functional theory (DFT). It is constructed from a self-interaction free exchange energy and a non-local correlation energy that directly accounts for dispersion.[*Eshuis et al.*, 2012a; *Ren et al.*, 2012a] The Random Phase Approximation (RPA) is the simplest approximation within ACFD-DFT and has proven to be a highly accurate method for treating weak interactions[*Björkman et al.*, 2012; *Eshuis and Furche*, 2011; *Harl and Kresse*, 2008a; *Lebègue et al.*, 2010; *Schimka et al.*, 2010a], predicting structural properties[*Burow et al.*, 2014; *Harl et al.*, 2010; *Olsen and Thygesen*, 2013a; *Patrick and Thygesen*, 2015a; *Peng and Lany*, 2013a] and energetics[*Patrick and Thygesen*, 2016; *Schimka et al.*, 2013b]. Although RPA captures intermediate and long-range correlation, it does not accurately account for the short-range correlation.[*Bates et al.*, 2016a; *Furche*, 2001a; *Ruzsinszky et al.*, 2010; *Yan et al.*, 2000] RPA was previously used to study the pressure-induced phase transitions of Si and SiO_2,

delivering an improvement over semilocal functionals for Si, but yielding mediocre results for SiO_2 likely due to an imperfect cancellation of errors.[*Xiao et al.*, 2012a] Recently, Cui *et al.* showed that the relative stability of TiO_2 in the rutile and anatase structure is correctly described by RPA. To establish a reliable benchmark method for all the materials, we need to go beyond RPA with minimal additional computational cost. Hence, to go beyond RPA, a kernel correction from time-dependent DFT or many-body perturbation theory must be included to correct the short-ranged behavior of RPA and improve the systematic performance of ACFD-based methods.[*Bates and Furche*, 2013a; *Grüneis et al.*, 2009; *Jansen et al.*, 2010a; *Olsen and Thygesen*, 2012,0] To assess the improvement, that ACFD-based methods may bring compared to semilocal functionals, we have investigated the phase induced transition pressures of several different materials described in the previous Chapter 2.

In the following sections, we briefly describe the applied methods and computational details in Section 3.2, and present the results for each system in Section 3.3. A brief discussion and conclusions are then given in Section 3.4.

3.2 Computational Details

The total energy within the ACFD-DFT formalism is obtained from the sum of a self-interaction error free exchange energy and the correlation energy,

$$E^{\mathrm{ACFD}} = E^{\mathrm{EXX}} + E_c^{\mathrm{ACFD}}\,. \tag{3.2-1}$$

The exact exchange (EXX) energy is equivalent to the Hartree-Fock energy evaluated with DFT orbitals[*Eshuis et al.*, 2012a; *Ren et al.*, 2012a], while the correlation energy E_c can be obtained exactly from knowledge of the interacting density-density response function[*Langreth and Perdew*, 1975a]. When necessary, we use the notation EXX@Functional to indicate the semilocal functional used in the non self-consistent

evaluation of the EXX energy. In practice, the interacting response function is obtained from approximate time-dependent(TD) DFT either within RPA or through the inclusion of an approximate xc-kernel, typically within the adiabatic approximation.[*Furche and Van Voorhis*, 2005; *Lein et al.*, 2000a] In this work we have explored both RPA and beyond-RPA (bRPA) methods to understand the importance of short-ranged correlation effects in predicting structural phase transitions. These methods also shed light on the balance of non-local exchange and correlation, and any fortuitous error cancellation exhibited by semilocal functionals. Since PBE reference orbitals are typically used to evaluate RPA, we have elected to use the spatially renormalized, adiabatic PBE exchange-like kernel[*Olsen and Thygesen*, 2014a] (rAPBE) to evaluate the bRPA contribution to the correlation energy.

In order to efficiently treat the bRPA correlation energy we utilize three approximations from RPA renormalized (RPAr) perturbation theory[*Bates and Furche*, 2013a; *Bates et al.*, 2016a,0]: first-order RPA renormalization (RPAr1), a higher-order terms (HOT) correction beyond RPAr1,[*Bates et al.*] and the ACSOSEX approximation[*Jansen et al.*, 2010a]. RPAr is based on the decomposition of the ground-state correlation energy into RPA and beyond-RPA correlation as,

$$E_c^{\mathrm{ACFD}} = E_c^{\mathrm{RPA}} + \Delta E_c^{\mathrm{bRPA}} . \tag{3.2-2}$$

The different methods mentioned above involve different approximations for $\Delta E_c^{\mathrm{bRPA}}$. RPAr offers a modest speedup compared to the traditional bRPA approach[*Langreth and Perdew*, 1977a] with a little loss in accuracy[*Bates et al.*, 2016a,0; *Colonna et al.*, 2014a]. The main difference between each bRPA method lies in the treatment of third and higher-order contributions to the many-body perturbation theory expansion of the correlation energy, though all three methods yield the exact second-order contribution if used with the exact kernel.[*Bates et al.*, 2016a] Since all three methods

require the computation of the RPA response function and the exchange-correlation kernel, they can be evaluated simultaneously with the RPA correlation energy once the kernel has been computed.[*Bates et al.*, 2017a]

RPAr1 has been previously used in tandem with an approximate exchange kernel[*Bates and Furche*, 2013a], the frequency-dependent exact exchange kernel[*Colonna et al.*, 2014a], and several approximate kernels from TDDFT[*Bates et al.*, 2017a], delivering high-accuracy without electronic instabilities in the response function.[*Bates and Furche*, 2013a; *Colonna et al.*, 2014a; *Olsen and Thygesen*, 2013b] Though several approximate kernels are available, the use of an exchange-like kernel should provide a general picture of the behavior of kernel corrections while keeping the computational cost close to RPA. Furthermore, advanced exchange-correlation kernels (non-linear in λ) did not yield significant differences compared to exchange-like kernels for structural properties of simple solids[*Patrick and Thygesen*, 2015a], though the discrepancies for energy differences are still an open question.

PBE orbitals were used as input for the ACFD methods since they are evaluated non-self consistently using a modified version of GPAW.[*Enkovaara et al.*, 2010; *Mortensen et al.*, 2005] Gamma-centered Monkhorst-Pack[*Monkhorst and Pack*, 1976] k-meshes were used throughout. For the beyond-RPA calculations the rAPBE kernel[*Olsen and Thygesen*, 2014a] was used with wave-vector symmetrization[*Patrick and Thygesen*, 2015a; *Trevisanutto et al.*, 2013] throughout. We have carefully done convergence tests for each material with the exact exchange (EXX), and the RPA correlation energy contribution with regards to the cutoff energy of the input wavefunctions and the k-mesh. All parameters were chosen to yield errors on the order of 0.02 eV per functional unit or less. The converged parameters we used are given by Table 3.1 below.

The EXX tends to be more difficult to converge, and typically requires larger cutoffs compared to semilocal functionals described in the previous Chapter 2.

Table 3.1: Convergence parameters used in our calculations of the transition pressures for ACFD methods.

Materials		**EXX**		**RPA**		**rAPBE**
	ecut(eV)	**k-mesh**	**ecut(eV)**	**k-mesh**	**ecut(eV)**	**k-mesh**
Si (Diamond)	800	10x10x10	350	8x8x8	350	6x6x6
Si (Beta-tin)	800	10x10x12	350	10x10x12	350	8x8x10
Ge (Diamond)	700	12x12x12	350	8x8x8	350	6x6x6
Ge (Beta-tin)	650	10x10x12	350	10x10x12	350	8x8x10
SiC (ZnS)	800	12x12x12	350	12x12x12	350	12x12x12
SiC (Rocksalt)	800	12x12x12	350	12x12x12	350	12x12x12
GaAs (ZnS)	600	6x6x6	300	6x6x6	300	6x6x6
GaAs (Cmcm)	600	8x7x9	275	6x5x7	275	4x3x5
SiO_2 (Quartz)	1000	4x4x2	550	2x2x1	550	2x2x1
SiO_2 (Stishovite)	1000	5x5x6	550	4x4x5	550	4x4x5
Pb (Fcc)	800	20x20x20	350	12x12x12	350	10x10x10
Pb (Hcp)	800	14x14x6	350	12x12x5	350	10x10x4
C (Graphite)	800	19x19x7	350	14x14x6	350	14x14x6
C (Diamond)	800	10x10x10	350	6x6x6	350	6x6x6
BN (Cubic)	1200	6x6x6	300	6x6x6	350	6x6x6
BN (Hexagonal)	950	8x8x3	300	8x8x3	350	8x8x3

Thereafter, we have used exact same numerical procedure as in Chapter 2 to find the zero-temperature phase transition pressure and phase transition pressure at a finite temperature using the phonon spectra. Although in principle the approximation used to compute E_{xc} for the electronic energy should also be used to compute the phonon spectra, this is not possible for ACFD functionals as well as for the SCAN meta-GGA in the previous chapter. Neither the analytic second derivatives of the potential energy with respect to the nuclear positions have been implemented in any code, nor performing finite differences would be reasonably expensive for the latter methods. In fact, only recently were the first derivatives for RPA implemented for periodic systems.[*Ramberger et al.*, 2017] Since we use PBE input orbitals for the ACFD methods, we have elected to use the phonon spectra predicted by PBE to compute all of the thermal effects for ACFD methods also in our work.

3.3 Results

Our results for the structural parameters of the materials, obtained with ACFD methods, are given by Table 3.2. For the ACFD methods, EXX overestimates the lattice constants as well as underestimates it without any systematic trend which might be due to neglect of correlation. Addition of correlation from RPA or bRPA methods typically improves the agreement with experiment, though the structural parameters tend to be overestimated. Consequently, the performance for the transition pressure shows a similar trend between semilocal and ACFD methods, though there are some differences for comparing performance across all the methods, as evident from Table 3.3 To compare the various ACFD methods we have studied the phase transition parameters of the same three groups of materials as for the semilocal case in the previous Chapter 2.

Table 3.2: Equilibrium cell volumes (Å^3) obtained from the EOS fits for each method. ACFD methods tend to overestimate by various degrees compared to the experiment.

Materials	**EXX**	**RPA**	**RPAr1**	**HOT**	**ACSOSEX**	**Expt**[1]
Si (Diamond)	41.348	40.460	40.744	40.663	40.507	40.037
Si (Beta-tin)	63.652	61.489	61.082	60.793	60.447	55.820[*McMahon et al.*, 1994]
Ge (Diamond)	44.966	46.073	46.368	46.314	46.102	45.271
Ge (Beta-tin)	76.133	75.037	74.908	74.617	74.169	
SiC (ZnS)	20.759	21.003	20.993	20.944	20.817	20.693
SiC (Rocksalt)	15.757	16.599	16.565	16.521	16.403	16.554[*Catti*, 2001b]
GaAs (ZnS)	45.448	46.854	47.097	47.073	46.923	45.138
GaAs (Cmcm)	151.868	154.077	152.393	151.640	150.435	
SiO_2 (Quartz)	40.881	37.939	38.478	38.528	38.594	37.803
SiO_2 (Stishovite)	22.799	23.896	23.922	23.895	23.711	23.325
Pb (Fcc)	34.190	29.726	30.556	30.535	30.471	30.010
Pb (Hcp)	68.916	59.250	60.929	60.875	60.686	48.530
C (Diamond)	11.132	11.373	11.336	11.312	11.228	11.345
C (Graphite)	34.381	35.436	35.618	35.227	34.966	36.615
BN (Cubic)	11.563	11.780	11.764	11.744	11.660	11.664
BN (Hexagonal)	35.478	36.266	36.387	36.367	36.110	36.701

Equilibrium energies are given in Table 3.4 below.

Table 3.3: Transition pressure (GPa) without temperature correction using ACFD methods.

Materials	**EXX**	**RPA**	**RPAr1**	**HOT**	**ACSOSEX**	**Expt**[*Mujica et al.*, 2003]
Si	51.4	13.8	11.4	10.7	11.1	12.0
Ge	51.1	11.2	10.4	10.1	10.9	10.6
SiC	114.6	74.3	71.4	70.3	71.0	100.0
GaAs	60.2	18.9	17.2	17.0	17.5	15.0
SiO_2	12.8	3.7	6.6	6.9	6.8	7.5[*Hamann*, 1996]
Pb	31.3	19.0	16.7	16.5	16.1	14.0
C	7.8	0.6	6.7	6.7	6.8	3.7
BN	10.8	–1.5	0.9	1.1	1.2	5.0

Table 3.4: Equilibrium energy differences without temperature corrections, reported in eV/functional unit using ACFD methods.

Materials	**EXX**	**RPA**	**RPAr1**	**HOT**	**ACSOSEX**
Si	1.260	0.384	0.334	0.317	0.328
SiC	2.662	1.655	1.606	1.583	1.599
Ge	1.046	0.276	0.267	0.262	0.280
GaAs	2.362	0.990	0.952	0.946	0.978
SiO_2	1.092	0.2488	0.508	0.535	0.542
Pb	0.041	0.035	0.027	0.026	0.027
C	0.145	0.012	0.129	0.130	0.130
BN	0.405	–0.057	0.038	0.044	0.048

3.3.1 Phase transitions between highly symmetric phases

Considering the first group of materials of Si, Ge and SiC and ACFD methods at zero temperature, Table 3.3 illustrates that EXX@PBE yields a very large overestimate of the transition pressures that is directly linked to its large overestimate of the energy difference between phases in both materials. Adding correlation from RPA significantly reduces the error of EXX and results in only slight overestimates of the transition pressures, which are further reduced by the addition of bRPA correlation from rAPBE with any of the RPAr approximations. The bRPA results are consequently slight underestimates in comparison to the experiment and the resulting errors are are quite close to one another,and comparable to RPA but with the opposite sign. We have seen for Si and Ge that the bRPA methods with the rAPBE

Table 3.5: Transition pressures (GPa) including temperature corrections at room temperature, 300 K using ACFD methods.

Materials	**RPA**	**RPAr1**	**HOT**	**Expt**[*Mujica et al.*, 2003]
Si	12.8	10.4	9.7	12.0
Ge	10.2	9.5	9.2	10.6
SiC	69.6	66.8	65.6	100.0
GaAs	18.0	16.3	16.0	15.0
SiO_2[1]	4.3	7.1	7.4	7.5[*Hamann*, 1996]
Pb	23.9	22.7	22.5	14.0
C	4.2	10.4	10.4	3.7
BN	1.8	4.3	4.4	5.0

kernel yield the most accurate results compared to the corresponding experiments, so we will use the RPAr1 value as a "reference" for SiC in future in this chapter. We note that the choice of RPAr method makes little difference since they all lie within approximately 1 GPa of each other. In this way, the analysis for Si and Ge is completely transferrable to SiC and hence why we have grouped them together; For SiC, while EXX is a drastic overestimate, RPA greatly reduces the error of EXX but still slightly overestimates compared to the bRPA methods.

With the addition of finite temperature corrections from the computed phonon spectra of PBE, the transition pressures for Si, Ge, and SiC, all shift to smaller values indicating a stability of the high-temperature phase in each case similar to the semilocal case depicted in the previous Chapter 2, as shown in Table 3.5. The shifts are fairly small here, and do not significantly change the relative trend amongst the functionals. RPA is now closest to the experiment for Si and Ge among the ACFD-based methods, and the bRPA methods yield slightly larger underestimates. For SiC, RPA still remain close to the bRPA methods.

3.3.2 Transitions involving a low-symmetry phase

For the second group of materials of GaAs and SiO_2, an accurate treatment of correlation at all ranges can be necessary to produce accurate results, though the

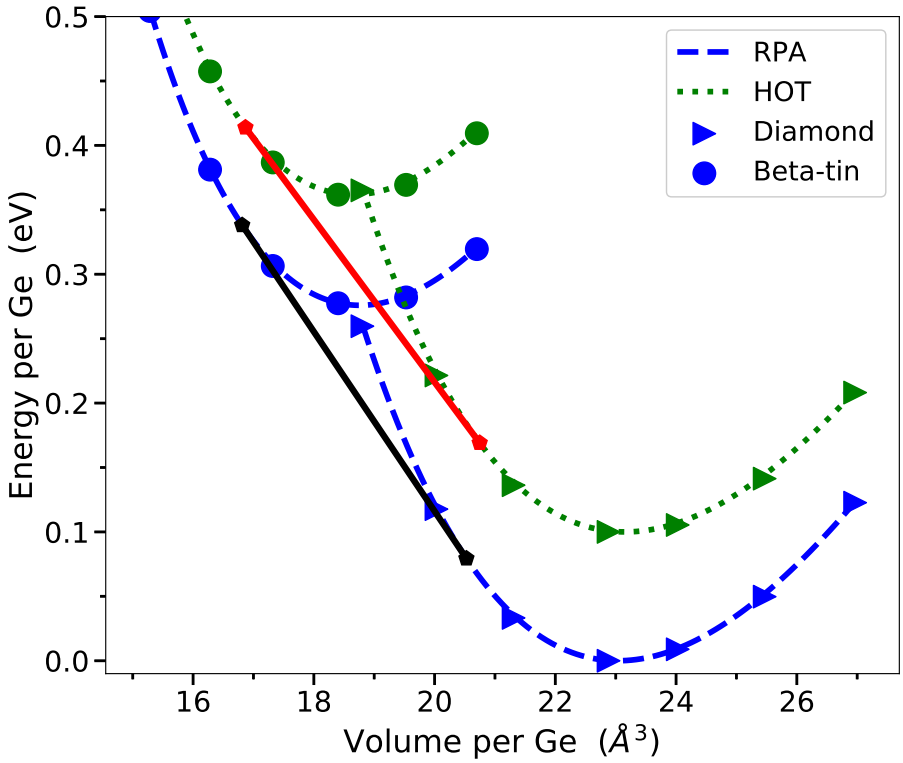

Figure 3.1: EV curve for diamond and betatin phases of Ge with RPA and bRPA per functional unit. The kernel corrections for Ge decrease slightly the equilibrium energy difference of the phases and hence slightly underestimate the transition pressure compared to RPA. The kernel-corrected curves have been rigidly shifted up in energy by 0.1 eV compared to RPA for visual clarity.

details of the electronic structure are also important. The ACFD methods show an analogous trend to the first group with EXX greatly overestimating the transition pressure due to its repulsive nature. With the addition of RPA correlation, the transition pressure drops down to a reasonable value but still overestimates in comparison to the experiment. Adding bRPA correlation from rAPBE at any level of RPAr again reduces the transition pressure of RPA and comes quite close to the experiment. For GaAs, bRPA methods are much closer to the experiment than RPA, though all of those methods are within 2 GPa of one another.

Fortunately, the ACFD methods are self-interaction free in the exchange energy,

but it is clear from Tables 3.3 and 3.4 that correlation still makes a huge impact on the results for SiO_2, since EXX overestimates the equilibrium energy difference and transition pressure by nearly a factor of two. As before, RPA correlation tames the wild error of EXX, but in this case results in an underestimate of the equilibrium energy difference and transition pressure by nearly the same factor that EXX overestimates. Our energy difference and transition pressure for RPA are smaller than those reported by Xiao *et al.*[*Xiao et al.*, 2012a], though the general trend compared to experiment is consistent. Ref. [*Xiao et al.*, 2012a] attributes this failure of RPA to its poor performance for some molecular-like solids where there is less cancellation of error between dissimilar phases. Looking at the difference between RPA and bRPA results, the root of the RPA error clearly stems from the inaccurate treatment of short-ranged correlation which can be improved through the inclusion of an exchange-correlation kernel correction.

The addition of the rAPBE corrections to RPA with any approximation of RPAr subsequently increases the equilibrium energy difference and transition pressure by raising the energy per SiO_2 of stishovite by approximately 260 meV more than it raises the energy of quartz, see Fig. 3.2. The resulting theoretical energy difference and transition pressure are increased compared to RPA and are consequently some of the most accurate data reported to date for this material, surpassing even the HSE06 screened-hybrid results reported in Ref. [*Xiao et al.*, 2013].

The comparison of ACFD-based methods is unlike that for the previous materials, since RPA struggles due to its inherent limitations, while the bRPA methods continue to deliver high-quality phase transition parameters since they are one-electron SIE free[*Ruzsinszky et al.*, 2007], and treat correlation correctly at all ranges of electron-electron interactions. Similar results are expected for other many-body bRPA methods such as SOSEX[*Grüneis et al.*, 2009] or AXK[*Bates and Furche*, 2013a] since they also tend to be one-electron, but not many-electron SIE free.[*Henderson and Scuse-*

ria, 2010a; *Ruzsinszky et al.*, 2007] The addition of thermal corrections for GaAs and SiO_2 is also similar to that for the first group in that the thermal corrections typically introduce only a rigid shift in the performance of all the ACFD methods. For GaAs the finite-temperature corrections reduce the transition pressures while for SiO_2 they increase the pressure and energy difference mostly due to entropic effects.[*Lee and Gonze*, 1995; *Xiao et al.*, 2013] These shifts neither change the relative relationships between functionals nor the experiment, and are not necessarily crucial for these materials where the energy gap between phases is appreciable.

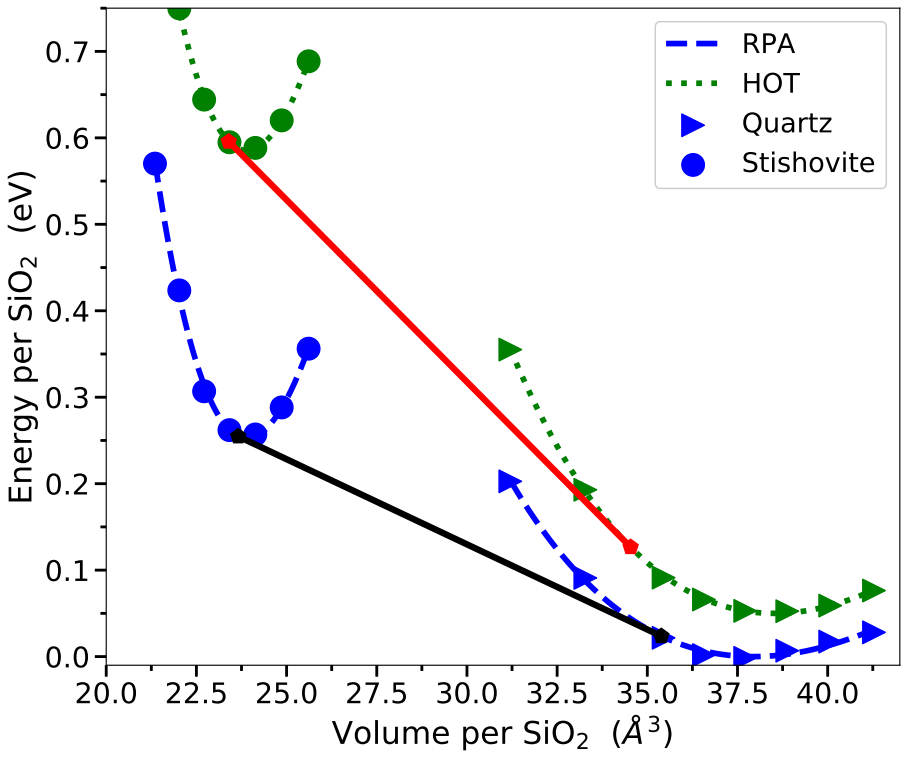

Figure 3.2: EV curve for quartz and stishovite phases of SiO_2 with RPA and bRPA per functional unit. The kernel corrections for SiO_2 increase the equilibrium energy difference of the phases and hence correct the large underestimation of the transition pressure by RPA. The kernel-corrected curves have been rigidly shifted up in energy by 0.05 eV compared to RPA for visual clarity.

3.3.3 Special cases

The third group of materials consisting of Pb, C and BN, are those for which there are some special circumstances which cause unexpected results or for which near degeneracies make it suitable to go beyond the semilocal functionals to the higher order ACFD methods. For Pb, a heavy Group IV element, relativistic effects can play an important role in determining the electronic structure as we learned in the earlier chapter. EXX@PBE fails spectacularly yet again, yielding roughly triple the experimental value. The addition of correlation from RPA reduces the roughly 20 GPa error of EXX down to about 4 GPa, but is still an overestimate compared to experiment, Table 3.3. The bRPA corrections reduce the transition pressure predicted by RPA by 1-2 GPa, further decreasing the error but still resulting in overestimates of the experimental value. Comparing the ACFD methods, RPA systematically overestimates by a slightly larger margin than bRPA methods.

Though non-relativistic methods are entirely appropriate for carbon and boron nitride materials, the near degeneracies at 0 K encountered for the cubic and hexagonal phases of these materials complicate predictions of the pressure induced phase transitions as discussed in the previous Chapter 2. All of the methods produce reasonably accurate structures for both phases of C and BN, but the predictions for the relative stabilities and transition pressures prove to be challenging for some of the methods. EXX yields a surprisingly reasonable result for the transition pressure of C, being only about 1.5 GPa larger than that predicted by semilocal PBE, though it yields a significantly larger transition pressure for BN than the semilocal functionals that we tested in the previous Chapter 2.

The performance of the correlated methods for C and BN is noticably different than for the previous materials as well. Earlier RPA calculations indicated nearly degenerate phases for carbon in the diamond and graphite phases[*Harl and Kresse*, 2009], and our results also confirm this behavior by the simplest ACFD correlation

method. Addition of beyond-RPA correlation, however, increases the energy difference between phases, by raising the energy of graphite relative to diamond and yielding transition pressures at zero-temperature that are overestimates in comparison to the finite-temperature experiments. We double checked that this large shift is not unique to the rAPBE kernel by applying the rALDA kernel[*Olsen and Thygesen*, 2013b]. The results were indeed very close to the rAPBE ones in Tables 3.3 and 3.4. Thus without access to other efficient exchange-correlation kernels at this time, it is difficult to understand why these two kernels generate such a large shift in the result of RPA correlation for carbon. For BN, however, RPA fails to predict the proper phase ordering, see Fig. 3.3. The addition of bRPA correlation from rAPBE corrects this deficiency and produces a small positive energy difference and transition pressure between the cubic and hexagonal phases. Since BN involves heteronuclear bonds, an accurate treatment of short-ranged correlation is likely needed to obtain good results, which we are able to achieve with the rAPBE kernel at any level of RPA renormalization, whereas for carbon the natural cancellation of errors of RPA results in an accurate result. For these two materials it is difficult to select one among the ACFD methods that is most accurate since the errors are similar in magnitudes though with differing signs. But taking account of the accurate relative stability of the different phases, bRPA outperforms RPA in terms of consistency and reliability.

The addition of thermal corrections for Pb, C, and BN tends to unilaterally destabilize the high-pressure phase resulting in a positive shift to the zero-temperature transition pressures, just like the semilocal case in the Chapter 2. For Pb, which is typically considered a very soft metal, the thermal corrections from PBE unilaterally result in overestimates of the finite-temperature transition pressure for all ACFD methods, though the spread in the results is noticably decreased. Thus it is clear that the zero-temperature results benefit from cancellation of opposing effects generated by the stabilization due to relativity and destabilization due to phonons in the HCP

phase. For C and BN at finite-temperature, RPA is quite close to experiment for the former but not the latter, while the bRPA methods are more accurate for BN than for C.

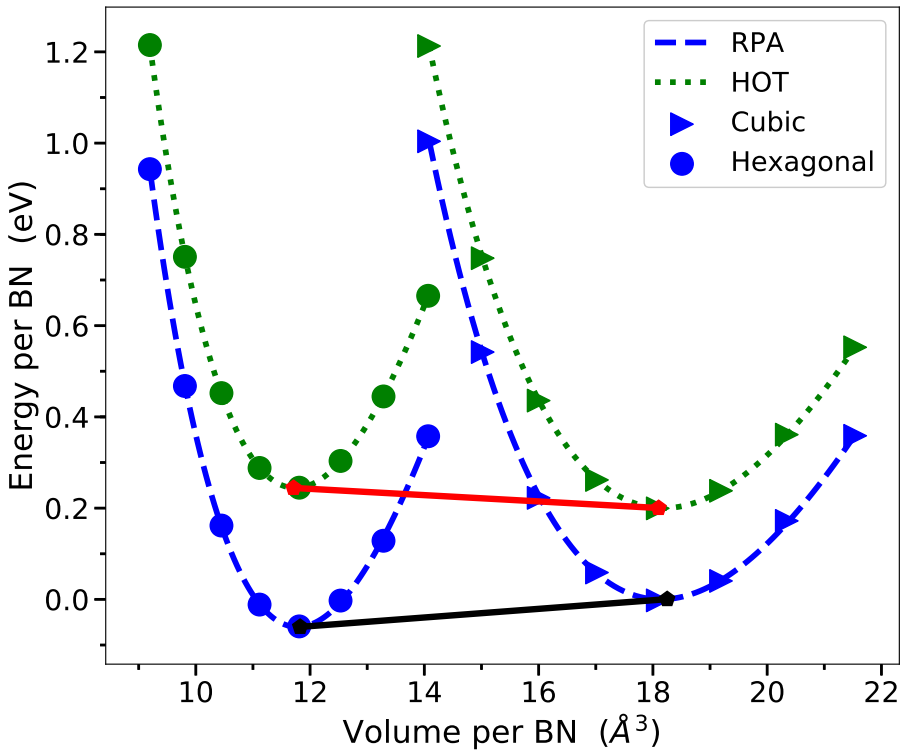

Figure 3.3: EV curve for cubic and hexagonal phases of BN with RPA and RPA with kernel correction per functional unit. Accounting for beyond-RPA correlation through an exchange-correlation kernel for BN changes the sign of the relative energy difference between the phases and hence corrects the errors of RPA. The kernel-corrected curves have been rigidly shifted up in energy by 0.2 eV compared to RPA for visual clarity.

3.3.4 Comparison with semilocal functionals

Figure 3.4 summarizes the finite-temperature results at 300 K and illustrates the relative performance of the selected methods with respect to the experiment. It is also a comparative analysis of semilocal functionals and ACFD methods. SCAN tends to be the most accurate semilocal functional and yields results in good agreement with

RPA. Overall, the thermally corrected bRPA methods yield consistent accuracy for all materials. The small differences between RPAr methods also indicate that the details of the bRPA method are not crucial, just that one must account for beyond-RPA correlation in a non-perturbative way as to avoid divergences for small-gap systems.

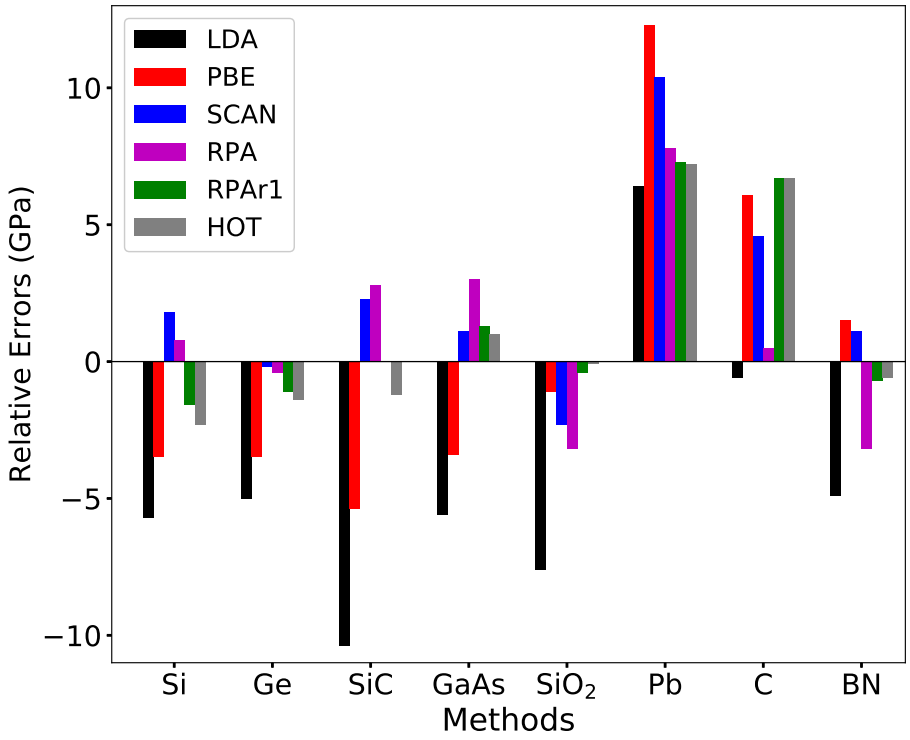

Figure 3.4: Relative errors (GPa) compared to experiment of the transition pressures at room temperature predicted by each method for each system. As explained in the text, the RPAr1 value is used as the reference value for SiC instead of the experimental result.

3.4 Discussions and Conclusions

We evaluated the performance of RPA, and beyond-RPA methods from RPA renormalization using the rAPBE exchange-like kernel in a comparative study for the determination of structural properties and transition parameters of different phases. Both the zero-temperature electronic structure calculations of the ground state and the finite-temperature predictions with thermal corrections from the phonons were

compared with experimental results. For materials with two high-symmetry phases and an appreciable energy difference between phases, semilocal density functionals are usefully accurate and the improvements from the ACFD methods are not substantial. The ACFD methods tend to improve upon the semilocal functionals for GaAs, though the inherent limitations of RPA can still result in poor results for molecular-like systems such as silica. For materials which require special consideration to understand their behavior, the ACFD methods tend to produce the most consistent results, though SCAN can also be a practical choice in these materials for compromising between speed and accuracy.

In general, methods such as rAPBE@RPAr1 should yield the most consistent results across all types of materials. Based on a self-interaction free exchange energy, bRPA methods accurately treat long-range interactions because they are based upon RPA correlation, as well as being accurate for short-ranged interactions due to the explicit inclusion of an exchange-correlation kernel. Since all length scales of the electron-electron interaction are accounted for systematically, one can expect the results produced by bRPA methods to be intrinsically accurate and not relying on cancellation of errors as is the case for semilocal functionals. Furthermore, higher-orders of RPAr do not make a large contribution to the phase transition parameters, since the difference between the HOT method and RPAr1 tends to be negligible. But we can conclude that bRPA methods can be used as quality control for both energy differences and transiton pressures whenever accurate experimental results are unavailable.

One point not discussed explicitly thus far is that the difference in behavior of exchange and correlation in semilocal functionals and ACFD methods is striking. For the former, the exchange potential and energy often comprise the majority of the binding described by density functional approximations, and the addition of the correlation potential and energy often induce only a (relatively) small shift from the

exchange-only results. For the ACFD, however, non self-consistent EXX typically underbinds by a considerable degree resulting in wildly inaccurate results. Thus the addition of correlation leads to very large shifts in the exchange-only results, in direct contrast to semilocal correlation. This difference in behavior is directly linked to the non-local nature of the EXX, and even though the exchange-only starting point is often nowhere close to experiment, the non-local correlation from the ACFD corrects this deficiency and yields the missing binding needed to produce accurate results. Thus we find the ACFD approach to be vital in the validation of semilocal results and recommend its use in materials where experimental results cannot be straightforwardly compared to other approximate electronic structure calculations. Also bRPA methods systematically improves RPA results, whereas, adding empirical long-range dispersions to the semilocal functionals does not always improve the results in a systematic way as specially evident in case of Boron Nitride and Silica in our study.

CHAPTER 4

ROLE OF FINITE ORDER VS. INFINITE ORDER KERNEL CORRECTIONS IN PHASE ORDERING AND INTERLAYER BINDING ENERGIES

4.1 Introduction

In this chapter, we have studied the role of finite order vs. infinite order kernel corrections in phase ordering and interlayer binding energies.[*Bates et al.*]

The Random Phase Approximation (RPA) has established iteself as an increasingly common Density Functional Approximation[*Hohenberg and Kohn*, 1964; *Kohn and Sham*, 1965] (DFT) based on the adiabatic connection fluctuation dissipation theorem.[*Eshuis et al.*, 2012b; *Langreth and Perdew*, 1977b; *Ren et al.*, 2012b] RPA is itself the simplest approximation within the adiabatic connection fluctutation-dissipation (ACFD) theorem formulation of DFT[*Furche*, 2001b; *Furche and Van Voorhis*, 2005; *Langreth and Perdew*, 1975b], which is an exact formulation of the correlation energy. Since the ACFD approach accounts for density fluctuations, dispersion interactions are naturally included. ACFD methods are also inherently self-interaction error free in their exchange energies, thus the ACFD is a straightforward route to eliminating two major challenges of approximate semilocal density functionals.[*Eshuis et al.*, 2012b; *Paier et al.*, 2012; *Ren et al.*, 2012b] The drawback of these improvements is the increased computational cost associated with the algorithms for evalu-

ating the correlation energy, however the difference in formal scaling between ACFD and semilocal DFT calculations can be made very close with recent implementations.[*Del Ben et al.*, 2013; *Eshuis et al.*, 2010; *Kállay*, 2015; *Kaltak et al.*, 2014; *Moussa*, 2014; *Wilhelm et al.*, 2016] RPA has been demonstrated to deliver improved predictions compared to the semilocal functionals and it is used to evaluate thermochemistry, structural properties, and weak-interactions.[*Bao et al.*, 2015; *Bates et al.*, 2016c; *Björkman et al.*, 2012; *Burow et al.*, 2013; *Harl and Kresse*, 2008b,0; *Karlicky et al.*, 2013; *Lebègue et al.*, 2010; *Mezei et al.*, 2015; *Olsen and Thygesen*, 2013d; *Peng and Lany*, 2013b; *Schimka et al.*, 2010b,0; *Waitt et al.*, 2016; *Xiao et al.*, 2012b; *Yan and Nørskov*, 2013] In spite of the accuracy of RPA for a wide range of problems, there are situations where it is unable to deliver high accuracy. Non-isogyric processes that break the number of electron pairs are one such class of energy differences where RPA struggles due to its improper treatment of short-ranged correlation.[*Fuchs et al.*, 2005; *Jiang and Engel*, 2007; *Mussard et al.*, 2015; *Pines and Bohm*, 1952] Beyond-RPA (bRPA) methods are needed in such cases, and within the ACFD formalism they can be easily obtained through the introduction of an exchange-correlation (xc) kernel from time-dependent DFT within the Dyson equation for the interacting density response function.[*Ángyán et al.*, 2011; *Bates and Furche*, 2013b; *Furche and Van Voorhis*, 2005; *Hesselmann and Görling*, 2010; *Lein et al.*, 2000b] Approaches to include exchange effects beyond RPA have also been developed from Coupled Cluster (CC) and other wavefunction theories,[*Lotrich and Bartlett*, 2011] due to the connection between CC doubles and the adiabatic connection.[*Jansen et al.*, 2010b; *Scuseria et al.*, 2008] The most widely used methods include SOSEX,[*Grüneis et al.*, 2009; *Henderson and Scuseria*, 2010b] and AC-SOSEX.[*Bates and Furche*, 2013b; *Bates et al.*, 2016b; *Dixit et al.*, 2017; *Jansen et al.*, 2010b] SO-SEX and AC-SOSEX are closely related, and the latter one can be cast as an approximation to the first-order RPA renormalized perturbation theory developed in Ref. [*Bates and Furche*, 2013b]. In

this chapter, we will focus on corrections from xc kernels within the ACFD. Many xc kernels have been suggested in the literature,[*Bates and Furche*, 2013b; *Bates et al.*, 2016b; *Constantin and Pitarke*, 2007; *Corradini et al.*, 1998; *Gould*, 2012; *Heßelmann and Görling*, 2011; *Lein et al.*, 2000b; *Lu*, 2014; *Olsen and Thygesen*, 2012,0] and the major distinction between most of them is whether they are derived from a model system such as the electron gas, or from many-body theory[*Grüneis et al.*, 2009]. A further distinction is based on the coupling-strength dependence. For exchange-like kernels uniform coordinate scaling shows these are linear in the coupling-strength, while for exchange-correlation kernels the dependence is non linear.[*Lein et al.*, 2000b] Herein we will make use of several exchange-like kernels originating from models of the homogeneous electron gas (HEG), since they were demonstrated to yield accurate structural properties and energy differences at a fraction of the cost of an exchange-correlation kernel calculation for bulk solids.[*Jauho et al.*, 2015; *Olsen and Thygesen*, 2013c; *Patrick and Thygesen*, 2015b] The spatially renormalized adiabatic DFT (rADFT) kernels[*Olsen and Thygesen*, 2012,0] are among the simplest exchange-like kernels available and will be combined with the ACFD herein to study both model and real systems. Without utilizing the traditional ACFD approach for computing the bRPA correlation energy, RPA renormalized[*Bates and Furche*, 2013b; *Bates et al.*, 2016b,0] (RPAr) perturbation theory was shown to deliver a robust treatment of bRPA correlation with several advantages compared to the infinite-order method. For exchange-like kernels an analytic integral exists for the first-order (RPAr1) correction.[*Bates and Furche*, 2013b; *Bates et al.*, 2016b] RPAr1 also guarantees the elimination of divergences due to electronic instabilities.[*Bates and Furche*, 2013b; *Colonna et al.*, 2014b; *Olsen and Thygesen*, 2013d] Compared to the infinite-order method, we showed previously that RPAr1 systematically underestimates the bRPA correction by approximately 10%,[*Bates et al.*, 2016b] which can be straightforwardly accounted for through the inclusion of higher-orders in the RPAr series.[*Bates et al.*, 2017b] The

drawback of higher-orders in the series is that an analytic coupling-strength integral is not currently known for those terms and thus the coupling-strength integration must be reintroduced just to compute a small fraction of the energy. To circumvent the coupling-strength integration entirely, we have developed a higher- order terms (HOT) approximation that seeks to account for the missing correlation beyond RPAr1. By studying the coupling-strength dependence of second and higher orders of RPAr in the electron gas, as well as the kinetic and potential contributions to correlation for the interacting system at full-coupling, we find that a one-parameter expression for the bRPAr1 correlation reproduces the infinite-order result to within about 1%. When the HOT approximation accurately reproduces the infinite-order bRPA correlation for a given system and kernel, structural properties and energy differences are also accurate. For open-shell systems our approximation is less robust, but we are able to understand the origin of this deficiency in terms of the behavior of the RPAr series in these cases. In Sec. 4.2 we discuss the computational details, whereas in Sec. 4.3 and Sec. 4.4 we provide results and discussions.

4.2 Computational Details

In keeping with our previous naming conventions,[*Bates et al.*, 2016b,0] when a given kernel is referenced directly as a correlation method we mean the infinite-order method. The acronym XACFD is also used to mean the exact ACFD correlation for a given kernel. While there are no analytical proof of the convergence of the RPAr series, it was demonstrated numerically that the finite-order RPAr correlation expansion does tend to converge to the exact result in both model and real solids, as well as for several finite systems.[*Bates et al.*, 2017b] Additionally the convergence is found to be monotonic from below for the systems in that study because each correction was positive and smaller than the previous order. This trend was rooted in an analytical analysis of the correlation potential that shows RPA renormalization systematically

sums subsets of terms in many-body perturbation theory (MBPT) that all have the same signed contribution to the correlation energy.[*Bates et al.*, 2017b] This is quite impressive for a perturbation expansion since traditional MBPT expansions based on non-interacting references are not gauranteed to converge at higher-orders and the convergence is not necessarily monotonic.[*Cremer and He*, 1996; *Laidig et al.*, 1985; *Manby and Knowles*, 2000; *Seidl et al.*, 2000]

For RPA and RPAr1 with exchange-like kernels the coupling-strength integration can be performed analytically so it is counter-productive to evaluate higher-orders exactly for real systems because numerical integrations of coupling strength are required. To avoid this, an accurate approximation can be obtained from a second-order correction to the response function which accounts for all higher-order terms(HOT).[*Bates et al.*, 2016b] For spin-nonpolarized systems, or spin-independent kernels, the coupling strength integral for the correlation energy of RPAr1 can be taken analytically for exchange-like kernels, meaning only one diagonalization of the response function at full coupling strength is needed to compute the correlation energy, thus avoiding instabilities that come from diagonalization of a response function that directly includes kernel.[*Bates and Furche*, 2013b; *Bates et al.*, 2017b; *Colonna et al.*, 2014b] The reduction in computational cost for periodic boundary conditions is related to the reduced amount of time needed for above diagonalization of the interacting response function in the reciprocal lattice basis, which is not rate-determining as the cost to build the noninteracting response function is quartic in a plane-wave basis. However, for systems such as metals where dense k-mesh samplings are needed for converged results, the reduction can be appreciable since the savings is per q-point. Exchange-correlation kernels or spin-polarized systems with any kernel still require numerical integration over coupling strength within RPAr as implemented using the density-density response function, so there is no reduction in computational cost, however instabilities are still avoided since only the interacting response function needs to be

diagonalized. As stressed in Ref. [*Bates et al.*, 2017b], within RPAr, the RPA and beyond RPA corrections are obtained simultaneously and one does not need to perform two separate calculations in order to determine the behavior of each method. Instead, the total energy is a sum of separate pieces and the impact of the kernel compared to RPA can be directly determined.

Though we have utilized a periodic boundary implementation, for molecular systems, the savings introduced by avoiding the repeated diagonalization of the RPA response function (or supermatrix[*Furche*, 2001b]) is actually significant. The diagonalization of matrices in the particle-hole basis scales as N^6 , where N is a measure of the basis set size, and the diagonalization must be carried out for every coupling-strength point used to integrate the correlation energy (typically between 6 and 8 points). Thus one is able to avoid repeatedly performing the rate-determining step by eliminating the numerical integration over the coupling strength. If the electron repulsion integrals are constructed using resolution of the identity methods in an integral-direct fashion, the cost to perform a HOT calculation via numerical integration of the frequency along the imaginary axis will be the same as that for RPA[*Burow et al.*, 2013; *Eshuis et al.*, 2010; *Grundei and Burow*, 2017] or RPAr1[*Bates and Furche*, 2013b], approximately O(N^4) with a prefactor that depends on the details of the implementation.

Using a modified version of the GPAW code,[*Bahn and Jacobsen*, 2002; *Mortensen et al.*, 2005; *Walter et al.*, 2008] we have implemented the HOT approximation in conjunction with the spin-dependent (rADFT) and spin-independent (rADFTns) forms of the exchange-like kernels rALDA[*Olsen and Thygesen*, 2012] and rAPBE[*Olsen and Thygesen*, 2014b]. When necessary we use the notation RPAr@kernel to denote which kernel has been used with a particular RPA renormalization approximation. The rALDA and rAPBE kernels have been demonstrated to improve upon RPA for energy differences and structural properties, and preserve the accurate description

of dispersion interactions for atoms, molecules, and solids.[*Jauho et al.*, 2015; *Olsen and Thygesen*, 2012,0,0; *Patrick and Thygesen*, 2015b] Since the combination of these kernels and RPAr resulted in analogous trends, here we will focus almost solely on the rAPBE kernel.

In addition to specifying the kernel within GPAW, one must specify a reciprocal lattice vector basis averaging scheme to compute the kernel since there are multiple ways to extend homogeneous electron gas kernels to inhomogeneous systems[*Lu*, 2014; *Olsen and Thygesen*, 2012; *Patrick and Thygesen*, 2015b; *Trevisanutto et al.*, 2013]. We have used the so-called wavevector symmetrization throughout to ensure that the kernel is symmetric in the reciprocal lattice basis because of its computational advantages, as discussed in Ref. [*Patrick and Thygesen*, 2015b]. There is the added bonus that the wavevector symmetrization also preserves the proper divergence behavior of the kernel in the $q \to 0$ limit.[*Patrick and Thygesen*, 2015b] See Ref. [*Patrick and Thygesen*, 2015b] for an overview of the averaging schemes. Calculations were performed within the projector-augmented wave formalism[*Blöchl*, 1994] using the 0.9.20000 GPAW datasets. Results for real systems were obtained using PBE orbitals to construct the Kohn-Sham reference determinant, and gamma-centered Monkhorst-Pack k-point meshes[*Monkhorst and Pack*, 1976] were used throughout. The maximum cutoff for the response function was chosen between 300 and 400 eV, the number of bands was chosen to be equal to the number of plane-waves, and the perturbative approach from Ref. [*Yan et al.*, 2011] was used to treat the divergence of the Coulomb interaction at small wavevectors. The frequency integral was performed using a 16 point Gauss-Legendre quadrature, and with a frequency scale of 2 for non-metals, and 2.5 for metals[*Harl and Kresse*, 2008b; *Olsen and Thygesen*, 2013d]. Extrapolation of the correlation energies to the basis set limit were performed using the Harl-Kresse[*Harl and Kresse*, 2008b] method with at least four cutoffs below the maximum. The cutoff used to generate the wavefunctions for the response

function was 600 eV. Fermi-Dirac occupations corresponding to an electronic temperature of 0.01 eV were used for all periodic systems. A Wigner-Seitz truncation scheme[*Sundararaman and Arias*, 2013] was used to treat the small wavevector divergence of the Coulomb interaction in the exchange energy. For atomic and molecular systems we used rectangular boxes with unequal side lengths to break spatial symmetry, and extrapolated the correlation energy from calculations at plane-wave cutoffs of 250 and 300 eV for the response function. These cutoffs were previously shown to deliver small errors compared to extrapolations with higher cutoffs for RPA.[*Olsen and Thygesen*, 2013d] Larger plane-wave cutoffs, box sizes, or volume based extrapolations of the correlation energy[*Harl and Kresse*, 2008b] would be needed to obtain fully converged results for each kernel, however the relative performance of RPAr to the infinite-order method is usually independent of the basis for cutoffs larger than 250 eV. For atoms, a larger variation in finite cutoff and extrapolated values can result in slower convergence of RPAr for the extrapolated results. For molecules and bulk systems the differences between the finite cutoff and extrapolated results tend to be negligible for any k-mesh and cutoffs above 200 eV. Results for the electron gas were obtained using an in-house python code. Gauss-Legendre quadratures of 12-20 points were used for the frequency and coupling-strength integration, while the q-integration is implemented using the rectangle method over $0 < q \leq 15$ a.u. with 3000 points.

4.3 Results

4.3.1 Binding energies

At first, we want to see the effects of both finite order renormalized bRPA methods and the infinite order XACFD, with the rAPBE kernel along with RPA on the interlayer binding energies of Molybdenum Di-Sulphide (MoS_2), Graphite (C) and

hexagonal Boron Nitride (h-BN), and compare it to the calculated binding energies of two weakly bound dimers ammonia and water. The results are given in the following Table 4.1.

Table 4.1: Binding energies (kcal/mol) for the ammonia and water dimers from the S22 test set, and inter-layer binding energy for MoS_2, graphite and h-BN (meV/$\mathring{A}^2$). Reference values were taken from Takatani et al. [*Takatani et al.*, 2010] for the S22 dimers, and from Ref. [*Björkman et al.*, 2012] for MoS_2, grahite, h-BN .

Materials	**EXX**	**RPA**	**RPAr1**	**HOT**	**XACFD**	**Ref.**
$(NH_3)_2$	1.14	2.02	2.99	4.52	3.12	3.15
$(H_2O)_2$	3.81	3.28	4.24	6.21	4.46	5.07
MoS_2	–14.9	22.4	20.8	20.8	21.9	20.5
Graphite	–13.10	17.89	18.16	18.37	18.45	24[*Wang et al.*, 2015]
h-BN	–15.19	12.91	12.74	12.85	12.87	-

For the molecular dimers, RPAr1 agrees with the infinite-order results (XACFD) to within 0.5 kcal/mol, but addition of the HOT approximation grossly overestimates the total binding energy due to a poor cancellation of errors. The binding energy of MoS_2, graphite, h-BN , on the other hand, is accurately reproduced by the HOT method since it involves bulk-like energy differences. In these dimers, the error in the total correlation energy for both the monomer and dimer is roughly equal, but of opposite sign. As a result, the errors do not cancel, and the HOT approximation yields interaction energies that are too large in comparison to the infinite-order method. This behavior can be traced back to the approximate value of parameter b to 0.5 for both systems, which results in a beyond RPAr1 correction that is too large for the dimers and too small for the monomers. Fortunately for these systems, however, RPAr1 recovers the dominant beyond-RPA contribution to the binding energy and yields a small error compared to the infinite-order method.

To understand the challenge facing the HOT method for these energy differences, Figure 4.1 shows the error of the HOT approximation in comparison to the infinite-order beyond RPAr1 correction as a function of HOT parameter $\hat{b}$ for the NH_3 dimer,

NH_3 monomer, and the binding energy. If $\hat{b}$ is chosen to be the same value for both NH_3 monomer and NH_3 dimer, then the value that yields the smallest error is close to 1, which represents RPAr1 without correction, since correlation energy of HOT is proportional to $(1-\hat{b})$. If $\hat{b}$ can be chosen independently for each system, the error in the binding energy is minimized when the error in the total correlation energies for each system is zero. A value of b = 0.55 for NH_3 monomer is needed to accomplish this, while a value of 0.5 was already quite accurate for the NH_3 dimer. The same challenge also applies to the cohesive and atomization energies or any other property measurement which includes both atoms and composites systems, since choosing one value of $\hat{b}$ for both atoms and composite systems is limited in accuracy due to poor cancellation of errors between the atomic errors and the bulk errors.

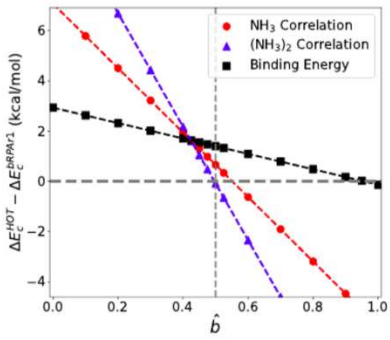

Figure 4.1: Correlation energy error of HOT compared to bRPAr1 as a function of HOT parameter $\hat{b}$ of individual NH_3 monomer, NH_3 dimer and their binding energies.

On the other hand, same cancellation of errors can also be found for the inter-

layer binding energy of MoS_2, graphite and h-BN. Dominated by the weak interaction between layers, the interlayer binding energy is difficult to predict with bare semilocal functionals and typically a dispersion correction is needed for accurate results.[*Björkman et al.*, 2012; *Peng et al.*, 2016] RPA has been used as a benchmark in these systems due to absence of high quality experimental data or other high level calculations,[*Björkman et al.*, 2012] yielding roughly 20 meV/$\mathring{A}^2$ for the binding energy of MoS_2. Our kernel-corrected calculations further confirm the accuracy of RPA for these systems since there is little difference between any of our RPAr results with rAPBE and the original RPA value. RPAr1 itself seems to capture all but 1 meV of the binding energy compared to the infinite-order method, and the addition of the HOT correction changes the RPAr1 result by very little. The error of the HOT approximation for mono and bilayer exhibits the same sign and so the error for the difference drops out yielding high fidelity to the XACFD result. Thus the HOT approximation is likely capable of predicting accurate exfoliation and surface properties since these involve differences of bulk-like structures. Furthermore, the adsorption of molecules on surfaces should also be accurately reproduced by the HOT approximation since both the surface and the molecule tend to be spin-unpolarized species and the HOT approximation is accurate in those cases.

4.3.2 Phase ordering

Though the HOT approximation struggles for energy differences describing fragmentation into monomer or atomic species, energy differences that involve only bulk or surface species can still be accurately reproduced. Two simple examples are the pressure induced phase transition between two phases of a material and the interlayer binding energy of MoS_2, graphite, h-BN. The transition pressure (P_t), at which the phase transition begins, can be computed from the common tangent between the EV curves of each material or through the equal enthalpy condition,

$H_1(V_1, P_t) = H_2(V_2, P_t)$, where $H(V, P) = E(V) + PV(P)$ is the enthalpy. Using a parametrized EOS to determine the energy as a function of volume and the volume as a function of pressure, P_t can be determined through numerical optimization. The biggest factors that determine the transition pressure are the energy and volume differences between phases since one can think of the common tangent as being $P_t(E_1 - E_2)/(V_1 - V_2)$ for the two phases. As an example of such a process, we have computed the transition pressure of Silicon Carbide from the zincblende (ZB) phase to the rocksalt (RS) phase. Both phases are semiconductors, and experimentally the transition pressure is observed to be on the order of 100 GPa, as discussed in Chapter 2 and Chapter 3. There we found that, semilocal functionals underestimate the experimental transition pressure due to a too small energy difference between the phases. A hybrid functional, such as B3LYP, increases the energy difference and subsequently the transition pressure between the phases due to the addition of exact exchange.[*Catti*, 2001b] RPA has been applied previously for other phase transitions, such as in Si[*Kaltak et al.*, 2014] and SiO_2[*Xiao et al.*, 2012b], however it does not always yield smaller errors in comparison to experiment. In such cases a kernel correction could improve the result, though this remains to be generally demonstrated. Here we use PBE input orbitals and the rAPBE kernel to evaluate RPAr1, HOT, and infinite-order methods. For the ZB→RS transition, the results are given in Table 4.2, for both the structural parameters and the transition pressure.

Though not discussed in previous reports of RPA transition pressures, the EXX and RPA correlation contributions to the transition pressure are often large and of opposite sign. In this case, EXX yields a transition pressure of 114 GPa and an energy difference of 2.66 eV/SiC between the phases, while the addition of RPA correlation reduces P_t by 40 GPa and the energy difference by 1 eV/SiC. Adding a kernel correction from RPAr yields a relatively small shift in the RPA results, reducing the transition pressure by 4 GPa and the energy difference by 0.07 eV/SiC. All of the

Table 4.2: Stabilized Jellium Equation of State (SJEOS)[*Alchagirov et al.*, 2001] parameters and phase transition parameters for the ZB→RS transition in SiC. $\Delta E_0 = E_0(RS) - E_0(ZB)$ at the equilibrium volume of each phase, P_t is the transition pressure, $\Delta V = (V_t(ZB) - V_t(RS))/V_t(ZB)$ is the percent reduction in volume at the transition, and V_t is the volume at the transition pressure computed for a given method. EXX yields a large estimate for the transition pressure, which is greatly reduced by the addition of RPA correlation. The addition of a kernel correction produces a relatively small shift from the RPA results.

Materials	**EXX**	**RPA**	**RPAr1**	**HOT**	**XACFD**	**Ref.**
Zincblende						
a ($\mathring{A}$)	4.363	4.380	4.379	4.376	4.375	4.36[1]
B_0 (GPa)	252	222	221	222	223	224[1]
B'_0	3.61	3.86	3.93	3.94	3.93	3.57[1]
Rocksalt						
a ($\mathring{A}$)	3.980	4.049	4.047	4.043	4.042	4.04[2]
B_0 (GPa)	372	287	289	292	293	252[2]
B'_0	3.73	3.87	3.88	3.87	3.87	3.26[2]
ΔE_0(eV/SiC)	2.66	1.65	1.61	1.58	1.58	-
P_t (GPa)	114	74	71	70	70	100[1]
ΔV (%)	19	18	18	18	18	20[1]
V_t(ZB) ($\mathring{A}^3$)	15.748	16.866	16.966	16.987	16.981	15.685[3]
V_t(RS) ($\mathring{A}^3$)	12.796	13.840	13.897	13.906	13.903	12.494[3]

kernel corrected methods yield essentially equivalent transition pressures and energy differences, though there is a 30 meV reduction in the energy difference from RPAr1 to HOT or the infinite-order method. Thus for this system it appears that the RPA results are quite acceptable for comparisons with experiment and the kernel introduces a relatively small shift. Though the predicted pressures appear too small in comparison to experiment, Ref. [*Lu et al.*, 2008] argues that the stiffness of this material leads to a larger experimental transition pressure in order to overcome the transition barrier. By performing phonon calculations as a function of pressure, Ref. [*Lu et al.*, 2008] reported that the ZB phase becomes unstable around 120 GPa, in better agreement with the experimental value. Looking at the performance of RPA renormalization, the first-order approximation already yields accurate transition pressure parameters compared to the infinite-order method. In contrast to the weak interactions in the

ammonia and water dimers, the accuracy of the HOT approximation quantitatively reproduces the infinite-order volume of each phase at the phase transition, the transition pressure, and the energy difference between phases. This is somewhat expected given the degree with which the HOT approximation is able to reproduce the EOS fits for the solids discussed above. The excellent performance of the HOT approximation for this type of energy difference stems from the consistent overestimation of the bRPAr1 correlation in each phase by approximately 30 meV. Since the error has the same sign in both phases it drops out when taking the energy difference, thus the HOT approximation is capable of reproducing energy differences between phases of SiC with high fidelity.

4.4 Discussions

In order to accurately treat short-ranged correlation within the ACFD, an exchange-correlation kernel should be added to RPA. RPA renormalization provides a systematic route to compute such corrections, with the added benefit that both RPA and beyond RPA contributions to the correlation energy can be computed simultaneously. To recover most part of infinite-order method RPAr1 is sufficient and sometimes adding higher-order terms(HOT) approximation almost recovers whole infinite-order contribution (XACFD). Though the HOT approximation struggles for energy differences describing fragmentation into monomer or atomic species, energy differences that involve only bulk or surface species can still be accurately reproduced. Two simple examples are the pressure induced phase transition between two phases of a material and the interlayer binding energy of MoS_2, graphite, h-BN, shown in this study.

Since experimental phase transition pressure of SiC is quite high (100 GPa), we have used SJEOS equation of state, which is more suitable for high pressure than Birch-Murnaghan(BM) equation of state in this study for finding the phase tran-

sition parameters of the ZB→RS transition in SiC. $\Delta E_0 = E_0(RS) - E_0(ZB)$ at the equilibrium volume of each phase, P_t is the transition pressure, $V = (V_t(ZB) - V_t(RS))/V_t(ZB)$ is the percent reduction in volume at the transition, and V_t is the volume at the transition pressure computed for a given method. EXX yields a large estimate for the transition pressure, which is greatly reduced by the addition of RPA correlation. The addition of a kernel correction produces a relatively small shift from the RPA results. For the missing correlation beyond RPAr1, we have used the HOT approximation to account for second-order and higher contributions from RPA renormalization. Though the HOT approximation is no longer a systematic underestimate of the beyond RPA correlation energy as is RPAr1, it delivers total correlation energies typically within 1% of the infinite-order method. Though the total correlation energy exhibits a small error, energy differences can be adversely affected by the non-systematic behavior of the HOT approximation. The weak interactions in two molecular dimers, exhibit a weak cancellation of errors between a composite system and its fragments. The HOT approximation quantitatively reproduces the structural parameters of several bulk solids, and the pressure induced phase transition of SiC from zincblende to rocksalt structures. If one is interested in accurate energy differences between composite systems, the HOT approximation will likely yield highly accurate results, but some caution is clearly due for open-shell systems. To remedy these issues one could imagine the fitting parameter $\hat{b}$ to minimize an error function, or by determining $\hat{b}$ as a function of spin-polarization.

CHAPTER 5

CONCLUSION

In Chapter 1 of our thesis, we have briefly described the theoretical methods used in our work. In Chapter 2, we have studied the structural phase transitions with semilocal density functionals along with long-range empirical dispersion corrections. In Chapter 3, we have studied the structural phase transitions with Adiabatic Connection Fluctuation Dissipation (ACFD) theorem based RPA and beyond RPA methods. In chapter 4, we have studied the effects of finite order HOT approximation with infinite-order XACFD method for a spatially renormalized rAPBE kernel with RPA renormalized response functions for interlayer binding energies and phase ordering. In this Conclusion chapter, we summarize our work of the whole thesis which is mainly constitued by Chapter 2, 3 and 4.

Among the three different groups of materials which we choose to represent phase transitions in materials in general as much as possible, all semilocal density functionals(LDA, PBE, SCAN) provide very accurate phase transition pressures compared to the experiment for the first group of materials with transition from highly symmetric to highly symmetric phases. Improvements due to RPA and bRPA methods compared to semilocal functionals are very negligible in this case. For second group of materials with atleast one lower symmetric phase involved, SCAN provides the best results in general among the semilocal functionals whereas RPA struggles for SiO_2 case which involves transition between two lower symmetric phases due to its inadequate description of short-range interactions. All the bRPA methods give very good results for these group of materials and improves RPA result significantly for SiO_2.

For the third group of materials involving phase transition between metallic phases of Pb and two energetically very close phases of materials C and BN, SCAN performs better than any other semilocal functionals we have used and bRPA methods again give most accurate results in general and significantly correct the inability of RPA for providing the correct phase ordering of BN at zero temperature. Now added empirical long-range dispersion corrections with semilocal functionals fail to improve the semilocal functional result systematically at zero temperature as evident in the case of SiO_2 and BN in our study. From this and RPA's severe underperformance to predict transition pressures between lower symmetric phases of SiO_2, we can derive the short and intermediate range interactions are more important for describing correct geometry of the phases and phase transition parameters in bulk solids compared to long range dispersions. Thermal corrections are needed not only to compare with the experimental results but we have found sometimes it is absolutely necessary to correct the wrong phase orderings of the functionals (LDA for C, BN and RPA for BN in our case). We have found that the kernel corrections in bRPA methods do always systematically improves RPA result of phase transition pressures for all three groups of materials whereas empirical dispersion corrections don't when applied on top of semilocal functionals. Also even first order RPAr1 can significantly improves the RPA result and higher order HOT method does not improve much on top of it. Without much more computational cost than RPA, bRPA methods can replace RPA as a benchmark methods for phase transition parameters calculation in future. By assessing the difference of finite order bRPA methods with the infinite order kernel correction method, we have found out that first order RPAr1 captures almost 90% of missing correlation correction of infinite order XACFD method. Hence, RPAr1 gives pretty close result to XACFD for both the binding energies of bulk like solids and molecular dimers as well as of phase transition parameters of bulk material SiC. On the otherhand, higer order approximation (HOT) method captures almost all of

remaining 10% of missing correlation of XACFD on top of RPAr1 for most cases. In case of the binding energies of bulk like solids and phase transition parameters of bulk SiC, it still improves RPAr1 by small margin compared to the infinite order XACFD results. However, it comes short for binding energies of molecular dimers providing somewhat large overestimation with respect to the results of XACFD methods owing to its inherent parametrization problem which leads to errors that do not cancel between a composite system and its constituent pieces for measuring energy differences involving fragmentation currently.

BIBLIOGRAPHY

Albe, K. (1997), Theoretical study of boron nitride modifications at hydrostatic pressures, *Phys. Rev. B*, *55*(10), 6203.

Alchagirov, A. B., J. P. Perdew, J. C. Boettger, R. C. Albers, and C. Fiolhais (2001), Energy and pressure versus volume: Equations of state motivated by the stabilized jellium model, *Phys. Rev. B*, *63*(22), 224,115.

Althoff, J. D., P. B. Allen, R. M. Wentzcovitch, and J. A. Moriarty (1993), Phase diagram and thermodynamic properties of solid magnesium in the quasiharmonic approximation, *Phys. Rev. B*, *48*(18), 13,253.

Ángyán, J. G., R. Liu, J. Toulouse, and G. Jansen (2011), correlation energy expressions from the adiabatic-connection fluctuation–dissipation theorem approach, *J. Chem. Theory Comput.*, *7*(10), 3116–3130.

Atkins, P., T. Overton, J. Rourke, M. Weller, and F. Armstrong (2010), *Shriver & Atkins' Inorganic Chemistry*, 5th ed ed., Oxford University Press.

Bachelet, G. B., and N. E. Christensen (1985), Relativistic and core-relaxation effects on the energy bands of gallium arsenide and germanium, *Phys. Rev. B*, *31*(2), 879.

Bahn, S. R., and K. W. Jacobsen (2002), An object-oriented scripting interface to a legacy electronic structure code, *Computing in Science & Engineering*, *4*(3), 56–66.

Baliga, B. J. (1989), Power semiconductor device figure of merit for high-frequency applications, *IEEE Electron Device Lett.*, *10*(10), 455–457.

Bao, J. L., H. S. Yu, K. Duanmu, M. A. Makeev, X. Xu, and D. G. Truhlar (2015), Density functional theory of the water splitting reaction on fe (0): Comparison of local and nonlocal correlation functionals, *ACS Catal.*, *5*(4), 2070–2080.

Baroni, S., S. De Gironcoli, A. Dal Corso, and P. Giannozzi (2001), Phonons and related crystal properties from density-functional perturbation theory, *Rev. Mod. Phys.*, *73*(2), 515.

Bates, J., N. Sengupta, J. Sensenig, and A. Ruzsinszky (), Adiabatic connection without coupling constant integration, *submitted in J. Chem. Theory Comput.*

Bates, J. E., and F. Furche (2013a), *J. Chem. Phys.*, *139*, 171,103.

Bates, J. E., and F. Furche (2013b), Communication: Random phase approximation renormalized many-body perturbation theory.

Bates, J. E., S. Laricchia, and A. Ruzsinszky (2016a), A non-local, energy-optimized kernel: Recovering second-order exchange in the homogeneous electron gas, *Phys. Rev. B*, *93*, 045,119.

Bates, J. E., S. Laricchia, and A. Ruzsinszky (2016b), Nonlocal energy-optimized kernel: Recovering second-order exchange in the homogeneous electron gas, *Phys. Rev. B*, *93*(4), 045,119.

Bates, J. E., P. D. Mezei, G. I. Csonka, J. Sun, and A. Ruzsinszky (2016c), Reference determinant dependence of the random phase approximation in 3 d transition metal chemistry, *J. Chem. Theory Comput.*, *13*(1), 100–109.

Bates, J. E., J. Sensenig, and A. Ruzsinszky (2017a), Convergence behavior of the random phase approximation renormalized correlation energy, *Phys. Rev. B*, *95*(19), 195,158.

Bates, J. E., J. Sensenig, and A. Ruzsinszky (2017b), Convergence behavior of the random phase approximation renormalized correlation energy, *Phys. Rev. B*, *95*(19), 195,158.

Besson, J. M., J. P. Itié, A. Polian, G. Weill, J. L. Mansot, and J. Gonzalez (1991), High-pressure phase transition and phase diagram of gallium arsenide, *Phys. Rev. B*, *44*(9), 4214.

Björkman, T., A. Gulans, A. V. Krasheninnikov, and R. M. Nieminen (2012), van der waals bonding in layered compounds from advanced density-functional first-principles calculations, *Phys. Rev. Lett.*, *108*, 235,502, 10.1103/PhysRevLett.108.235502.

Björkman, T., A. Gulans, A. V. Krasheninnikov, and R. M. Nieminen (2012), van der waals bonding in layered compounds from advanced density-functional first-principles calculations, *Phys. Rev. Lett.*, *108*(23), 235,502.

Blakemore, J. (1982), Semiconducting and other major properties of gallium arsenide, *J. Appl. Phys.*, *53*(10), R123–R181.

Blöchl, P. E. (1994), Projector augmented-wave method, *Phys. Rev. B*, *50*(24), 17,953.

Brandenburg, J., J. Bates, J. Sun, and J. Perdew (2016a), Benchmark tests of a strongly constrained semilocal functional with a long-range dispersion correction, *Physical Review B*, *94*(11), 115,144.

Brandenburg, J. G., J. E. Bates, J. Sun, and J. P. Perdew (2016b), Benchmark tests of a strongly constrained semilocal functional with a long-range dispersion correction, *Physical Review B*, *94*(11), 115,144.

Bundy, F., W. Bassett, M. Weathers, R. Hemley, H. Mao, and A. Goncharov (1996), The pressure-temperature phase and transformation diagram for carbon; updated through 1994, *Carbon*, *34*(2), 141–153.

Burow, A. M., J. E. Bates, F. Furche, and H. Eshuis (2013), Analytical first-order molecular properties and forces within the adiabatic connection random phase approximation, *J. Chem. Theory Comput.*, *10*(1), 180–194.

Burow, A. M., J. E. Bates, F. Furche, and H. Eshuis (2014), Analytical first-order molecular properties and forces within the adiabatic connection random phase approximation, *J. Chem. Theory Comput.*, *10*, 180–194.

Catti, M. (2001a), Orthorhombic intermediate state in the zinc blende to rocksalt transformation path of sic at high pressure, *Phys. Rev. Lett.*, *87*, 035,504, 10.1103/PhysRevLett.87.035504.

Catti, M. (2001b), Orthorhombic intermediate state in the zinc blende to rocksalt transformation path of sic at high pressure, *Phys. Rev. Lett.*, *87*(3), 035,504.

Ceperley, D. M., and B. Alder (1980), Ground state of the electron gas by a stochastic method, *Physical Review Letters*, *45*(7), 566.

Chang, K. J., and M. L. Cohen (1987), Ab initio pseudopotential study of structural and high-pressure properties of sic, *Phys. Rev. B*, *35*(15), 8196.

Colonna, N., M. Hellgren, and S. de Gironcoli (2014a), *Phys. Rev. B*, *90*, 125,150.

Colonna, N., M. Hellgren, and S. de Gironcoli (2014b), Correlation energy within exact-exchange adiabatic connection fluctuation-dissipation theory: Systematic development and simple approximations, *Phys. Rev. B*, *90*(12), 125,150.

Constantin, L. A., and J. M. Pitarke (2007), Simple dynamic exchange-correlation kernel of a uniform electron gas, *Phys. Rev. B*, *75*(24), 245,127.

Corradini, M., R. Del Sole, G. Onida, and M. Palummo (1998), Analytical expressions for the local-field factor g (q) and the exchange-correlation kernel k xc (r) of the homogeneous electron gas, *Phys. Rev. B*, *57*(23), 14,569.

Cremer, D., and Z. He (1996), Sixth-order møller- plesset perturbation theory on the convergence of the mp n series, *J. Phys. Chem.*, *100*(15), 6173–6188.

Crowe, T. W., R. J. Mattauch, H. Roser, W. L. Bishop, W. C. Peatman, and X. Liu (1992), Gaas schottky diodes for thz mixing applications, *Proc. IEEE*, *80*(11), 1827–1841.

Cui, Z.-H., F. Wu, and H. Jiang (2016), First-principles study of relative stability of rutile and anatase tio 2 using the random phase approximation, *Phys. Chem. Chem. Phys.*, *18*(43), 29,914–29,922.

Curtice, W. R. (1980), A mesfet model for use in the design of gaas integrated circuits, *IEEE Trans. Microw. Theory Tech.*, *28*(5), 448–456.

Dal Corso, A., A. Pasquarello, A. Baldereschi, and R. Car (1996), Generalized-gradient approximations to density-functional theory: A comparative study for atoms and solids, *Phys. Rev. B*, *53*(3), 1180.

Davis, R. F. (1991), Iii-v nitrides for electronic and optoelectronic applications, *Proceedings of the IEEE*, *79*(5), 702–712.

Del Ben, M., J. Hutter, and J. VandeVondele (2013), Electron correlation in the condensed phase from a resolution of identity approach based on the gaussian and plane waves scheme, *J. Chem. Theory Comput.*, *9*(6), 2654–2671.

Dion, M., H. Rydberg, E. Schröder, D. C. Langreth, and B. I. Lundqvist (2004), Van der waals density functional for general geometries, *Physical review letters*, *92*(24), 246,401.

Dixit, A., J. Claudot, S. Lebègue, and D. Rocca (2017), Improving the efficiency of beyond-rpa methods within the dielectric matrix formulation: Algorithms and applications to the a24 and s22 test sets, *J. Chem. Theory Comput.*, *13*(11), 5432–5442.

Durandurdu, M. (2007), Ab initio simulations of the structural phase transformation of 2 h-si c at high pressure, *Phys. Rev. B*, *75*(23), 235,204.

Eastman, D., W. Grobman, J. Freeouf, and M. Erbudak (1974), Photoemission spectroscopy using synchrotron radiation. i. overviews of valence-band structure for ge, gaas, gap, insb, znse, cdte, and agl, *Phys. Rev. B*, *9*(8), 3473.

Enkovaara, J., et al. (2010), Electronic structure calculations with gpaw: a real-space implementation of the projectoraugmented-wave method, *J. Phys. Condens. Matter*, *22*(25), 253,202.

Eshuis, H., and F. Furche (2011), *J. Phys. Chem. Lett.*, *2*, 983.

Eshuis, H., J. Yarkony, and F. Furche (2010), Fast computation of molecular random phase approximation correlation energies using resolution of the identity and imaginary frequency integration, *J. Chem. Phys.*, *132*(23), 234,114.

Eshuis, H., J. E. Bates, and F. Furche (2012a), *Theor. Chem. Acc.*, *131*, 1084.

Eshuis, H., J. E. Bates, and F. Furche (2012b), Electron correlation methods based on the random phase approximation, *Theor. Chem. Acc.*, *131*(1), 1084.

Fuchs, M., Y. M. Niquet, X. Gonze, and K. Burke (2005), Describing static correlation in bond dissociation by kohn–sham density functional theory, *J. Chem. Phys.*, *122*(9), 094,116.

Furche, F. (2001a), *Phys. Rev. B*, *64*, 195,120.

Furche, F. (2001b), Molecular tests of the random phase approximation to the exchange-correlation energy functional, *Phys. Rev. B*, *64*(19), 195,120.

Furche, F., and T. Van Voorhis (2005), Fluctuation-dissipation theorem density-functional theory, *J. Chem. Phys.*, *122*(16), 164,106, 10.1063/1.1884112.

Furche, F., and T. Van Voorhis (2005), Fluctuation-dissipation theorem density-functional theory, *J. Chem. Phys.*, *122*(16), 164,106.

Furthmüller, J., J. Hafner, and G. Kresse (1994), Ab initio calculation of the structural and electronic properties of carbon and boron nitride using ultrasoft pseudopotentials, *Phys. Rev. B*, *50*(21), 15,606.

Gaál-Nagy, K., A. Bauer, M. Schmitt, K. Karch, P. Pavone, and D. Strauch (1999), Temperature and dynamical effects on the high-pressure cubic-diamond β-tin phase transition in si and ge, *Phys. Status Solidi B*, *211*(1), 275–280.

Gobat, A., M. Lamorte, and G. McIver (1962), Characteristics of high-conversion-efficiency gallium-arsenide solar cells, *IEEE Trans. Mil. Electron.*, *1051*(1), 20–27.

Gonze, X., and C. Lee (1997), Dynamical matrices, born effective charges, dielectric permittivity tensors, and interatomic force constants from density-functional perturbation theory, *Phys. Rev. B*, *55*(16), 10,355.

Gould, T. (2012), Communication: Beyond the random phase approximation on the cheap: Improved correlation energies with the efficient radial exchange hole kernel.

Grimme, S. (2006), *J. Comput. Chem.*, *27*, 1787–1799.

Grimme, S., J. Antony, S. Ehrlich, and H. Krieg (2010), A consistent and accurate ab initio parametrization of density functional dispersion correction (dft-d) for the 94 elements h-pu, *J. Chem. Phys.*, *132*(15), 154,104.

Grimme, S., S. Ehrlich, and L. Goerigk (2011), *J. Comput. Chem.*, *32*, 1456–1465.

Grundei, M. M. J., and A. M. Burow (2017), Random phase approximation for periodic systems employing direct coulomb lattice summation, *J. Chem. Theory Comput.*, *13*(3), 1159–1175.

Grüneis, A., M. Marsman, J. Harl, L. Schimka, and G. Kresse (2009), Making the random phase approximation to electronic correlation accurate, *J. Chem. Phys.*, *131*, 154,115.

Grüneis, A., M. Marsman, J. Harl, L. Schimka, and G. Kresse (2009), Making the random phase approximation to electronic correlation accurate, *J. Chem. Phys.*, *131*(15), 154,115.

Haas, P., F. Tran, and P. Blaha (2009), Calculation of the lattice constant of solids with semilocal functionals, *Phys. Rev. B*, *79*(8), 085,104.

Hamann, D. R. (1996), Generalized gradient theory for silica phase transitions, *Phys. Rev. Lett.*, *76*, 660.

Hamdi, I., and N. Meskini (2010), Ab initio study of the structural, elastic, vibrational and thermodynamic properties of the hexagonal boron nitride: Performance of lda and gga, *Physica B: Condensed Matter*, *405*(13), 2785–2794.

Harl, J., and G. Kresse (2008a), *Phys. Rev. B*, *77*, 045,136.

Harl, J., and G. Kresse (2008b), Cohesive energy curves for noble gas solids calculated by adiabatic connection fluctuation-dissipation theory, *Phys. Rev. B*, *77*(4), 045,136.

Harl, J., and G. Kresse (2009), Accurate bulk properties from approximate many-body techniques, *Phys. Rev. Lett.*, *103*(5), 056,401.

Harl, J., L. Schimka, and G. Kresse (2010), *Phys. Rev. B*, *81*, 115,126.

Henderson, T. M., and G. E. Scuseria (2010a), The connection between self-interaction and static correlation: a random phase approximation perspective, *Mol. Phys.*, *108*, 2511.

Henderson, T. M., and G. E. Scuseria (2010b), The connection between self-interaction and static correlation: a random phase approximation perspective, *Mol. Phys.*, *108*(19-20), 2511–2517.

Hermann, A., J. Furthmüller, H. W. Gäggeler, and P. Schwerdtfeger (2010), Spin-orbit effects in structural and electronic properties for the solid state of the group-14 elements from carbon to superheavy element 114, *Phys. Rev. B*, *82*, 155,116, 10.1103/PhysRevB.82.155116.

Hesselmann, A., and A. Görling (2010), Random phase approximation correlation energies with exact kohn–sham exchange, *Mol. Phys.*, *108*(3-4), 359–372.

Heßelmann, A., and A. Görling (2011), Correct description of the bond dissociation limit without breaking spin symmetry by a random-phase-approximation correlation functional, *Phys. Rev. Lett.*, *106*(9), 093,001.

Hohenberg, P., and W. Kohn (1964), Inhomogeneous electron gas, *Phys. Rev.*, *136*(3B), B864.

Jain, A., et al. (2013), The Materials Project: A materials genome approach to accelerating materials innovation, *APL Materials*, *1*, 011,002, 10.1063/1.4812323.

Jansen, G., R.-F. Liu, and J. G. Ángyán (2010a), *J. Chem. Phys.*, *133*, 154,106.

Jansen, G., R.-F. Liu, and J. G. Ángyán (2010b), On the equivalence of ring-coupled cluster and adiabatic connection fluctuation-dissipation theorem random phase approximation correlation energy expressions, *The Journal of chemical physics*, *133*(15), 154,106.

Jauho, T. S., T. Olsen, T. Bligaard, and K. S. Thygesen (2015), Improved description of metal oxide stability: Beyond the random phase approximation with renormalized kernels, *Phys. Rev. B*, *92*(11), 115,140.

Jiang, H., and E. Engel (2007), Random-phase-approximation-based correlation energy functionals: Benchmark results for atoms, *J. Chem. Phys.*, *127*(18), 184,108.

Kállay, M. (2015), Linear-scaling implementation of the direct random-phase approximation, *J. Chem. Phys.*, *142*(20), 204,105.

Kaltak, M., J. Klimeš, and G. Kresse (2014), Cubic scaling algorithm for the random phase approximation: Self-interstitials and vacancies in si, *Phys. Rev. B*, *90*(5), 054,115.

Kang, Y., et al. (2014), Plasmonic hot electron induced structural phase transition in a mos2 monolayer, *Adv. Mater.*, *26*(37), 6467–6471.

Karch, K., P. Pavone, W. Windl, O. Schütt, and D. Strauch (1994), *Ab initio* calculation of structural and lattice-dynamical properties of silicon carbide, *Phys. Rev. B*, *50*, 17,054–17,063, 10.1103/PhysRevB.50.17054.

Karlicky, F., P. Lazar, M. Dubecky, and M. Otyepka (2013), Random phase approximation in surface chemistry: Water splitting on iron, *J. Chem. Theory Comput.*, *9*(8), 3670–3676.

Kashyap, A. S., et al. (2013), Silicon carbide integrated circuits for extreme environments, in *Wide Bandgap Power Devices and Applications (WiPDA), 2013 IEEE Workshop on*, pp. 60–63, IEEE.

Kato, A., M. Nishigaki, N. Mamedov, M. Yamazaki, S. Abdullayeva, E. Kerimova, H. Uchiki, and S. Iida (2003), Optical properties and photo-induced memory effect related with structural phase transition in tlgas 2, *J. Phys. Chem. Solids*, *64*(9), 1713–1716.

Kern, G., G. Kresse, and J. Hafner (1999), Ab initio calculation of the lattice dynamics and phase diagram of boron nitride, *Phys. Rev. B*, *59*(13), 8551.

Klimeš, J., D. R. Bowler, and A. Michaelides (2011), Van der waals density functionals applied to solids, *Physical Review B*, *83*(19), 195,131.

Kohn, W., and L. J. Sham (1965), Self-consistent equations including exchange and correlation effects, *Phys. Rev.*, *140*(4A), A1133.

Kohn, W., A. D. Becke, and R. G. Parr (1996), Density functional theory of electronic structure, *J. Phys. Chem.*, *100*(31), 12,974–12,980.

Kresse, G., and J. Hafner (1993), Ab initio molecular dynamics for liquid metals, *Phys. Rev. B*, *47*(1), 558.

Kresse, G., and D. Joubert (1999), From ultrasoft pseudopotentials to the projector augmented-wave method, *Phys. Rev. B*, *59*(3), 1758.

Laidig, W. D., G. Fitzgerald, and R. J. Bartlett (1985), Is fifth-order mbpt enough?, *Chem. Phys. Lett.*, *113*(2), 151–158.

Landerville, A., M. Conroy, M. Budzevich, Y. Lin, C. White, and I. Oleynik (2010), Equations of state for energetic materials from density functional theory with van der waals, thermal, and zero-point energy corrections, *Appl. Phys. Lett.*, *97*(25), 251,908.

Langreth, D. C., and M. Mehl (1981), Easily implementable nonlocal exchange-correlation energy functional, *Physical Review Letters*, *47*(6), 446.

Langreth, D. C., and J. P. Perdew (1975a), *Solid State Commun.*, *17*, 1425.

Langreth, D. C., and J. P. Perdew (1975b), The exchange-correlation energy of a metallic surface, *Solid State Commun.*, *17*(11), 1425–1429.

Langreth, D. C., and J. P. Perdew (1977a), *Phys. Rev. B*, *15*, 2884.

Langreth, D. C., and J. P. Perdew (1977b), Exchange-correlation energy of a metallic surface: Wave-vector analysis, *Phys. Rev. B*, *15*(6), 2884.

Lebègue, S., J. Harl, T. Gould, J. G. Ángyán, G. Kresse, and J. F. Dobson (2010), *Phys. Rev. Lett.*, *105*, 196,401.

Lebègue, S., J. Harl, T. Gould, J. G. Ángyán, G. Kresse, and J. F. Dobson (2010), Cohesive properties and asymptotics of the dispersion interaction in graphite by the random phase approximation, *Phys. Rev. Lett.*, *105*(19), 196,401.

Lee, C., and X. Gonze (1995), Ab initio calculation of the thermodynamic properties and atomic temperature factors of sio 2 α-quartz and stishovite, *Phys. Rev. B*, *51*(13), 8610.

Lein, M., E. K. U. Gross, and J. P. Perdew (2000a), *Phys. Rev. B*, *61*, 13,431.

Lein, M., E. K. U. Gross, and J. P. Perdew (2000b), Electron correlation energies from scaled exchange-correlation kernels: Importance of spatial versus temporal nonlocality, *Phys. Rev. B*, *61*(20), 13,431.

Liu, A. Y., A. Garca, M. L. Cohen, B. K. Godwal, and R. Jeanloz (1991), Theory of high-pressure phases of pb, *Phys. Rev. B*, *43*(2), 1795.

Lotrich, V., and R. J. Bartlett (2011), External coupled-cluster perturbation theory: Description and application to weakly interaction dimers. corrections to the random phase approximation, *J. Chem. Phys.*, *134*(18), 184,108.

Lu, D. (2014), Evaluation of model exchange-correlation kernels in the adiabatic connection fluctuation-dissipation theorem for inhomogeneous systems, *J. Chem. Phys.*, *140*(18), 18A520.

Lu, Y.-P., D.-W. He, J. Zhu, and X.-D. Yang (2008), First-principles study of pressure-induced phase transition in silicon carbide, *Physica B: Condens. Matter*, *403*(19), 3543–3546.

Mailhiot, C., and A. K. McMahan (1991), Atmospheric-pressure stability of energetic phases of carbon, *Phys. Rev. B*, *44*(21), 11,578.

Manby, F., and P. J. Knowles (2000), An exchange functional for accurate virtual orbital energies, *J. Chem. Phys.*, *112*(16), 7002–7007.

Mao, H., Y. Wu, J. Shu, J. Hu, R. Hemley, and D. Cox (1990), High-pressure phase transition and equation of state of lead to 238 gpa, *Solid State Commun.*, *74*(9), 1027–1029.

McMahon, M. I., R. J. Nelmes, N. G. Wright, and D. R. Allan (1994), Pressure dependence of the imma phase of silicon, *Phys. Rev. B*, *50*(2), 739.

Mejia-Rodriguez, D., and S. Trickey (2017), Deorbitalization strategies for meta-generalized-gradient-approximation exchange-correlation functionals, *Physical Review A*, *96*(5), 052,512.

Mezei, P. D., G. I. Csonka, and M. Kallay (2015), Accurate diels–alder reaction energies from efficient density functional calculations, *J. Chem. Theory Comput.*, *11*(6), 2879–2888.

Miao, M. S., and W. R. L. Lambrecht (2003), Unified path for high-pressure transitions of sic polytypes to the rocksalt structure, *Phys. Rev. B*, *68*, 092,103, 10.1103/PhysRevB.68.092103.

Minomura, S., and H. Drickamer (1962), Pressure induced phase transitions in silicon, germanium and some iii–v compounds, *J. Phys. Chem. Solids*, *23*(5), 451–456.

Moll, N., M. Bockstedte, M. Fuchs, E. Pehlke, and M. Scheffler (1995), Application of generalized gradient approximations: the diamond–β-tin phase transition in si and ge, *Phys. Rev. B*, *52*(4), 2550.

Monkhorst, H. J., and J. D. Pack (1976), Special points for brillouin-zone integrations, *Phys. Rev. B*, *13*(12), 5188.

Mori-Sánchez, P., A. J. Cohen, and W. Yang (2006), Many-electron self-interaction error in approximate density functionals, *J. Chem. Phys.*, *125*, 201,102.

Mortensen, J. J., L. B. Hansen, and K. W. Jacobsen (2005), Real-space grid implementation of the projector augmented wave method, *Phys. Rev. B*, *71*(3), 035,109.

Mounet, N., and N. Marzari (2005), First-principles determination of the structural, vibrational and thermodynamic properties of diamond, graphite, and derivatives, *Phys. Rev. B*, *71*(20), 205,214.

Moussa, J. E. (2014), Cubic-scaling algorithm and self-consistent field for the random-phase approximation with second-order screened exchange, *J. Chem. Phys.*, *140*(1), 014,107.

Mujica, A., A. Rubio, A. Munoz, and R. Needs (2003), High-pressure phases of group-iv, iii–v, and ii–vi compounds, *Rev. Mod. Phys.*, *75*(3), 863.

Mussard, B., P. Reinhardt, J. G. Ángyán, and J. Toulouse (2015), Spin-unrestricted random-phase approximation with range separation: Benchmark on atomization energies and reaction barrier heights, *J. Chem. Phys.*, *142*(15), 154,123.

Nelmes, R., and M. McMahon (1995), Ordered superstructure of insb-iv, *Phys. Rev. Lett.*, *74*(1), 106.

Olsen, T., and K. S. Thygesen (2012), Extending the random-phase approximation for electronic correlation energies: The renormalized adiabatic local density approximation, *Phys. Rev. B*, *86*(8), 081,103.

Olsen, T., and K. S. Thygesen (2013a), Random phase approximation applied to solids, molecules, and graphene-metal interfaces: From van der waals to covalent bonding, *Phys. Rev. B*, *87*, 075,111, 10.1103/PhysRevB.87.075111.

Olsen, T., and K. S. Thygesen (2013b), *Phys. Rev. B*, *88*, 115,131.

Olsen, T., and K. S. Thygesen (2013c), Beyond the random phase approximation: Improved description of short-range correlation by a renormalized adiabatic local density approximation, *Phys. Rev. B*, *88*(11), 115,131.

Olsen, T., and K. S. Thygesen (2013d), Random phase approximation applied to solids, molecules, and graphene-metal interfaces: From van der waals to covalent bonding, *Phys. Rev. B*, *87*(7), 075,111.

Olsen, T., and K. S. Thygesen (2014a), Accurate ground-state energies of solids and molecules from time-dependent density-functional theory, *Phys. Rev. Lett.*, *112*, 203,001, 10.1103/PhysRevLett.112.203001.

Olsen, T., and K. S. Thygesen (2014b), Accurate ground-state energies of solids and molecules from time-dependent density-functional theory, *Phys. Rev. Lett.*, *112*(20), 203,001.

Paier, J., X. Ren, P. Rinke, G. E. Scuseria, A. Grüneis, G. Kresse, and M. Scheffler (2012), Assessment of correlation energies based on the random-phase approximation, *New Journal of Physics*, *14*(4), 043,002.

Patrick, C. E., and K. S. Thygesen (2015a), *J. Chem. Phys.*, *143*, 102,802.

Patrick, C. E., and K. S. Thygesen (2015b), Adiabatic-connection fluctuation-dissipation dft for the structural properties of solidsthe renormalized alda and electron gas kernels, *J. Chem. Phys.*, *143*(10), 102,802.

Patrick, C. E., and K. S. Thygesen (2016), Hubbard-*u*corrected hamiltonians for non-self-consistent random-phase approximation total-energy calculations: A study of zn s, tio_2, and nio, *Phys. Rev. B*, *93*, 035,133, 10.1103/PhysRevB.93.035133.

Pavone, P., S. Baroni, and S. de Gironcoli (1998), α β phase transition in tin: A theoretical study based on density-functional perturbation theory, *Phys. Rev. B*, *57*(17), 10,421.

Peng, H., and S. Lany (2013a), Polymorphic energy ordering of mgo, zno, gan, and mno within the random phase approximation, *Phys. Rev. B*, *87*, 174,113, 10.1103/PhysRevB.87.174113.

Peng, H., and S. Lany (2013b), Polymorphic energy ordering of mgo, zno, gan, and mno within the random phase approximation, *Phys. Rev. B*, *87*(17), 174,113.

Peng, H., Z.-H. Yang, J. P. Perdew, and J. Sun (2016), Versatile van der waals density functional based on a meta-generalized gradient approximation, *Phys. Rev. X*, *6*(4), 041,005.

Perdew, J. P., and A. Zunger (1981a), Self-interaction correction to density-functional approximations for many-electron systems, *Phys. Rev. B*, *23*(10), 5048.

Perdew, J. P., and A. Zunger (1981b), Self-interaction correction to density-functional approximations for many-electron systems, *Physical Review B*, *23*(10), 5048.

Perdew, J. P., J. A. Chevary, S. H. Vosko, K. A. Jackson, M. R. Pederson, D. J. Singh, and C. Fiolhais (1992), Atoms, molecules, solids, and surfaces: Applications of the generalized gradient approximation for exchange and correlation, *Phys. Rev. B*, *46*(11), 6671.

Perdew, J. P., K. Burke, and M. Ernzerhof (1996a), Generalized gradient approximation made simple, *Phys. Rev. Lett.*, *77*(18), 3865.

Perdew, J. P., K. Burke, and M. Ernzerhof (1996b), Generalized gradient approximation made simple, *Physical review letters*, *77*(18), 3865.

Perdew, J. P., S. Kurth, A. Zupan, and P. Blaha (1999), Accurate density functional with correct formal properties: A step beyond the generalized gradient approximation, *Physical review letters*, *82*(12), 2544.

Perdew, J. P., K. Schmidt, V. Van Doren, C. Van Alsenoy, and P. Geerlings (2001), Jacobs ladder of density functional approximations for the exchange-correlation energy, in *AIP Conference Proceedings*, vol. 577, pp. 1–20, AIP.

Pines, D., and D. Bohm (1952), A collective description of electron interactions: Ii. collective vs individual particle aspects of the interactions, *Phys. Rev.*, *85*(2), 338.

Radaelli, P. G., G. Iannone, M. Marezio, H. Y. Hwang, S. W. Cheong, J. D. Jorgensen, and D. N. Argyriou (1997), Structural effects on the magnetic and transport properties of perovskite a 1- x a x mno 3 (x= 0.25, 0.30), *Phys. Rev. B*, *56*(13), 8265.

Ramberger, B., T. Schäfer, and G. Kresse (2017), Analytic interatomic forces in the random phase approximation, *Phys. Rev. Lett.*, *118*, 106,403, 10.1103/PhysRevLett .118.106403.

Rappoport, D., N. R. M. Crawford, F. Furche, and K. Burke (2006), *Approximate Density Functionals: Which Should I Choose?*, John Wiley & Sons, Ltd, 10.1002/ 0470862106.ia615.

Ren, X., P. Rinke, C. Joas, and M. Scheffler (2012a), Random-phase approximation and its applications in computational chemistry and materials science, *J. Mater. Sci.*, *47*, 7447–7471, 10.1007/s10853-012-6570-4.

Ren, X., P. Rinke, C. Joas, and M. Scheffler (2012b), Random-phase approximation and its applications in computational chemistry and materials science, *J. Mater. Sci.*, *47*(21), 7447–7471.

Ruzsinszky, A., J. P. Perdew, G. I. Csonka, O. A. Vydrov, and G. E. Scuseria (2007), Density functionals that are one- and two- are not always many-electron self-interaction-free, as shown for h2+, he2+, lih+, and ne2+, *J. Chem. Phys.*, *126*, 104,102, 10.1063/1.2566637.

Ruzsinszky, A., J. P. Perdew, and G. I. Csonka (2010), *J. Chem. Theory Comput.*, *6*, 127.

Sabatini, R., T. Gorni, and S. de Gironcoli (2013), Nonlocal van der waals density functional made simple and efficient, *Phys. Rev. B*, *87*(4), 041,108.

Schimka, L., J. Harl, A. Stroppa, A. Grüneis, M. Marsman, F. Mittendorfer, and G. Kresse (2010a), Accurate surface and adsorption energies from many-body perturbation theory, *Nat. Mater.*, *9*, 741–744, 10.1038/nmat2806.

Schimka, L., J. Harl, A. Stroppa, A. Grüneis, M. Marsman, F. Mittendorfer, and G. Kresse (2010b), Accurate surface and adsorption energies from many-body perturbation theory, *Nature Materials*, *9*(9), 741.

Schimka, L., R. Gaudoin, J. Klimeš, M. Marsman, and G. Kresse (2013a), Lattice constants and cohesive energies of alkali, alkaline-earth, and transition metals: Random phase approximation and density functional theory results, *Phys. Rev. B*, *87*(21), 214,102.

Schimka, L., R. Gaudoin, J. Klimeš, M. Marsman, and G. Kresse (2013b), Lattice constants and cohesive energies of alkali, alkaline-earth, and transition metals: Random phase approximation and density fun ctional theory results, *Phys. Rev. B*, *87*, 214,102, 10.1103/PhysRevB.87.214102.

Schmidt, T., and S. Kümmel (2016), The influence of one-electron self-interaction on d-electrons, *Computation*, *4*(3), 33.

Schwetz, K. (2000), Silicon carbide based hard materials, *Handbook of ceramic hard materials*, pp. 683–748.

Scuseria, G. E., T. M. Henderson, and D. C. Sorensen (2008), The ground state correlation energy of the random phase approximation from a ring coupled cluster doubles approach.

Seidl, M., J. P. Perdew, and S. Kurth (2000), Simulation of all-order density-functional perturbation theory, using the second order and the strong-correlation limit, *Phys. Rev. Lett.*, *84*(22), 5070.

Sengupta, N., J. E. Bates, and A. Ruzsinszky (), From semilocal density functionals to random phase approximation renormalized perturbation theory: A methodological assessment of structural phase transitions, *submitted in Phys. Rev. B*.

Shahi, C., J. Sun, and J. P. Perdew (2018), Accurate critical pressures for structural phase transitions of group iv, iii-v, and ii-vi compounds from the scan density functional, *Phys. Rev. B*, *97*(9), 094,111.

Solozhenko, V. L., V. Z. Turkevich, and W. B. Holzapfel (1999), Refined phase diagram of boron nitride, *J. Phys. Chem. B*, *103*(15), 2903–2905.

Sun, J., A. Ruzsinszky, and J. P. Perdew (2015), Strongly constrained and appropriately normed semilocal density functional, *Physical review letters*, *115*(3), 036,402.

Sun, J., et al. (2016), Accurate first-principles structures and energies of diversely bonded systems from an efficient density functional, *Nat. Chem.*, *8*(9), 831–836.

Sundararaman, R., and T. A. Arias (2013), Regularization of the coulomb singularity in exact exchange by wigner-seitz truncated interactions: Towards chemical accuracy in nontrivial systems, *Phys. Rev. B*, *87*(16), 165,122.

Takatani, T., E. G. Hohenstein, M. Malagoli, M. S. Marshall, and C. D. Sherrill (2010), Basis set consistent revision of the s22 test set of noncovalent interaction energies, *J. Chem. Phys.*, *132*(14), 144,104.

Tao, J., J. P. Perdew, V. N. Staroverov, and G. E. Scuseria (2003), Climbing the density functional ladder: Nonempirical meta–generalized gradient approximation designed for molecules and solids, *Physical Review Letters*, *91*(14), 146,401.

Tkatchenko, A., and M. Scheffler (2009), Accurate molecular van der waals interactions from ground-state electron density and free-atom reference data, *Physical review letters*, *102*(7), 073,005.

Trevisanutto, P. E., A. Terentjevs, L. A. Constantin, V. Olevano, and F. Della Sala (2013), Optical spectra of solids obtained by time-dependent density functional theory with the jellium-with-gap-model exchange-correlation kernel, *Phys. Rev. B*, *87*(20), 205,143.

Van Tuyl, R., V. Kumar, D. D'avanzo, T. Taylor, V. Peterson, D. Hornbuckle, R. Fisher, and D. Estreich (1982), A manufacturing process for analog and digital gallium arsenide integrated circuits, *IEEE Trans. Microw. Theory Tech.*, *30*(7), 935–942.

Vanderborgh, C. A., Y. K. Vohra, H. Xia, and A. L. Ruoff (1990), bcc lead at 109 gpa: Diffraction studies to 208 gpa, *Phys. Rev. B*, *41*(10), 7338.

Vel, L., G. Demazeau, and J. Etourneau (1991), Cubic boron nitride: synthesis, physicochemical properties and applications, *Materials Science and Engineering: B*, *10*(2), 149–164.

Vlasko-Vlasov, V. K., Y. K. Lin, D. J. Miller, U. Welp, G. W. Crabtree, and V. I. Nikitenko (2000), Direct magneto-optical observation of a structural phase transition in thin films of manganites, *Phys. Rev. Lett.*, *84*(10), 2239.

von Barth, U., and L. Hedin (1972), A local exchange-correlation potential for the spin-polarized case, *J. Phys. C*, *5*, 1629.

Vosko, S. H., L. Wilk, and M. Nusair (1980), Accurate spin-dependent electron liquid correlation energies for local spin density calculations: a critical analysis, *Canadian Journal of physics*, *58*(8), 1200–1211.

Vydrov, O. A., and T. Van Voorhis (2009), Nonlocal van der waals density functional made simple, *Physical review letters*, *103*(6), 063,004.

Vydrov, O. A., and T. Van Voorhis (2010), Nonlocal van der waals density functional: The simpler the better, *J. Chem. Phys.*, *133*(24), 244,103.

Waitt, C., N. M. Ferrara, and H. Eshuis (2016), Thermochemistry and geometries for transition-metal chemistry from the random phase approximation, *J. Chem. Theory Comput.*, *12*(11), 5350–5360.

Walter, M., H. Häkkinen, L. Lehtovaara, M. Puska, J. Enkovaara, C. Rostgaard, and J. J. Mortensen (2008), Time-dependent density-functional theory in the projector augmented-wave method, *J. Chem. Phys.*, *128*(24), 244,101.

Wang, W., S. Dai, X. Li, J. Yang, D. J. Srolovitz, and Q. Zheng (2015), Measurement of the cleavage energy of graphite, *Nature communications*, *6*.

Weir, S. T., Y. K. Vohra, C. A. Vanderborgh, and A. L. Ruoff (1989), Structural phase transitions in gaas to 108 gpa, *Phys. Rev. B*, *39*(2), 1280.

Wentzcovitch, R. M., S. Fahy, M. L. Cohen, and S. G. Louie (1988), Ab initio study of graphite diamondlike transitions in bn, *Phys. Rev. B*, *38*(9), 6191.

Whittleton, S. R., A. Otero-de-la Roza, and E. R. Johnson (2017), The exchange-hole dipole dispersion model for accurate energy ranking in molecular crystal structure prediction, *J. Chem. Theory Comput.*

Wilhelm, J., P. Seewald, M. Del Ben, and J. Hutter (2016), Large-scale cubic-scaling random phase approximation correlation energy calculations using a gaussian basis, *J. Chem. Theory Comput.*, *12*(12), 5851–5859.

Xiao, B., J. Sun, A. Ruzsinszky, J. Feng, and J. P. Perdew (2012a), *Phys. Rev. B*, *86*, 094,109.

Xiao, B., J. Sun, A. Ruzsinszky, J. Feng, and J. P. Perdew (2012b), Structural phase transitions in si and sio 2 crystals via the random phase approximation, *Phys. Rev. B*, *86*(9), 094,109.

Xiao, B., J. Sun, A. Ruzsinszky, J. Feng, R. Haunschild, G. E. Scuseria, and J. P. Perdew (2013), Testing density functionals for structural phase transitions of solids under pressure: Si, sio 2, and zr, *Phys. Rev. B*, *88*(18), 184,103.

Yan, J., and J. K. Nørskov (2013), Calculated formation and reaction energies of 3 d transition metal oxides using a hierarchy of exchange-correlation functionals, *Phys. Rev. B*, *88*(24), 245,204.

Yan, J., J. J. Mortensen, K. W. Jacobsen, and K. S. Thygesen (2011), Linear density response function in the projector augmented wave method: Applications to solids, surfaces, and interfaces, *Phys. Rev. B*, *83*(24), 245,122.

Yan, Z., J. P. Perdew, and S. Kurth (2000), *Phys. Rev. B*, *61*, 16,430.

Yin, M. T., and M. L. Cohen (1982), Theory of static structural properties, crystal stability, and phase transformations: Application to si and ge, *Phys. Rev. B*, *26*(10), 5668.

Yoshida, M., A. Onodera, M. Ueno, K. Takemura, and O. Shimomura (1993), Pressure-induced phase transition in sic, *Phys. Rev. B*, *48*(14), 10,587.

Zhang, Y., and W. Yang (1998), A challenge for density functionals: Self-interaction error increases for systems with a noninteger number of electrons, *J. Chem. Phys.*, *109*(7), 2604–2608.

Zhao, Y., and D. G. Truhlar (2008), The m06 suite of density functionals for main group thermochemistry, thermochemical kinetics, noncovalent interactions, excited states, and transition elements: two new functionals and systematic testing of four

m06-class functionals and 12 other functionals, *Theoretical Chemistry Accounts*, *120*(1-3), 215–241.